Geological Society, London, Memoirs

# Chapter 15 Compositional variations of magmas in the Aeolian arc: implications for petrogenesis and geodynamics

A. Peccerillo, G. De Astis, D. Faraone, F. Forni and M. L. Frezzotti

*Geological Society, London, Memoirs* 2013, v.37; p491-510.
doi: 10.1144/M37.15

# Chapter 15

# Compositional variations of magmas in the Aeolian arc: implications for petrogenesis and geodynamics

A. PECCERILLO[1*], G. DE ASTIS[2], D. FARAONE[1], F. FORNI[3] & M. L. FREZZOTTI[4]

[1]*Dipartimento di Scienze della Terra, Università di Perugia, Piazza Università 1, 06100 Perugia, Italy*

[2]*INGV (Istituto Nazionale di Geofisica e Vulcanologia), Sezione di Sismologia e Tettonofisica, Via di Vigna Murata 605, 00143 Roma, Italy*

[3]*Dipartimento di Scienze Biologiche, Geologiche e Ambientali, Alma Mater Studiorum, Università di Bologna, Piazza Porta S.Donato 1, 40126 Bologna, Italy*

[4]*Dipartimento di Scienze dell'Ambiente e del Territorio e di Scienze della Terra, Università di Milano – Bicocca, Piazza Della Scienza 4, 20126 Milano, Italy*

**Corresponding author (e-mail: angelo.peccerillo@unipg.it)*

**Abstract:** The volcanic rocks of the Aeolian arc exhibit important within-island and along-arc compositional variations that testify to both geochemical heterogeneous mantle sources and different roles and intensities of shallow-level magmatic evolution processes. Calc-alkaline magmas are present on all islands, but dominate in the western arc and at Lipari and Panarea. Shoshonitic rocks are present on the central-eastern islands and are particularly abundant at Vulcano and Stromboli. Mafic and intermediate rocks comprise the bulk of older volcanic sequences for most islands. Rhyolites are restricted to younger activity of the central arc, and become particularly abundant at Lipari and Vulcano. Regional variations of incompatible trace element ratios and Sr-, Nd-, and Pb-isotope signatures in mafic-intermediate rocks document the variable composition of mantle sources, which were contaminated by different types of metasomatic fluids released from an oceanic slab in the western-central sectors and from oceanic slab plus sediments in the east. This metasomatism was superimposed over a heterogeneous mantle wedge, which had a mid-ocean-ridge basalt (MORB-) to ocean-island basalt (OIB)-type character passing from the centre to the margins of the arc. The OIB-type component in the external arc is attributed to asthenospheric mantle inflow from the Africa foreland, around the borders of a narrow slab during rollback.

Aeolian arc magmatism (Fig. 15.1) exhibits strong within-island and regional variations in elemental and isotopic compositions. These are the integrated effects of a variety of different processes that include heterogeneity of the mantle sources, variable physico-chemical conditions during magma formation and complex geochemical evolution during magma ascent to the surface (e.g. Keller 1982; Francalanci *et al.* 1989, 2004, 2007; Peccerillo 2005).

Intra-crustal magma compositional evolution was the latest process to occur and therefore left the best evidence in the petrological and geochemical signatures of subaerial volcanic rocks. Much more difficult to understand are the compositional characteristics and conditions of melting within mantle wedge. This is generally accomplished by studying the compositions of mafic magmas erupted along the arc, based on the assumption that these are reliable proxies of their mantle sources. However, it has been demonstrated that complex evolution processes in the Aeolian arc also affected mafic magmas which, in some cases, are more heavily contaminated by wall rocks than the coexisting intermediate magmas (see Peccerillo & Wu 1992; Peccerillo *et al.* 1993, 2004; Santo *et al.* 2004; Lucchi *et al.* 2013*a*). This makes the understanding of source composition and evolution processes a particularly challenging problem, which is still a subject of debate.

This paper is a critical review of the petrology and geochemistry of the Aeolian arc magmatism and of current ideas regarding the origin and evolution of magmas, mantle source compositions and their geodynamic significance. The paper consists of two parts. The first part is based on literature data and summarizes the volcanological and structural setting of the arc, describes the first-order compositional variation of rocks in the single islands and at the regional scale and discusses the nature and effects of magma evolution processes. The second part deals with regional variations of trace elements and radiogenic isotope compositions of magmas and their mantle sources and discusses the most popular hypotheses regarding mechanisms and effects of mantle metasomatism, conditions of formation of shoshonitic and calc-alkaline magmas and the geodynamic setting of the Aeolian arc. Along-arc geochemical variations are examined based upon new LAICPMS (Laser Ablation Inductively Coupled Plasma Mass Spectrometry) trace element analyses for a large number of representative samples from across the Aeolian arc. Intermediate rocks are considered along with mafic rocks, since andesites from some islands show the most primitive isotopic compositions across the arc and therefore represent more reliable proxies of mantle sources than mafic rocks. The new analyses provide an internally consistent set of data that overcomes the problems of inter-laboratory analytical bias, a main limitation of data in the literature. These data offer a better insight into fine-scale regional geochemical zoning, thus providing a foundation for development of a comprehensive model of the mantle source composition and its geodynamic significance.

## Structural, volcanological and petrological outlines

The Aeolian volcanism consists of seven main islands (Alicudi, Filicudi, Salina, Lipari, Vulcano, Panarea and Stromboli) making up a volcanic arc and several seamounts (Marsili, Eolo, Enarete, Sisifo, Lametini, Alcione, and Palinuro). These have formed around and inside the Masili basin (Fig. 15.1), a rapidly expanding back-arc basin (Nicolosi *et al.* 2006) floored by basaltic rocks and characterized by thin lithosphere and crust (Trua *et al.* 2004). The arc exhibits strong lateral variation of structural, volcanological and petrological characteristics, which make the Aeolian volcanoes an important case study for subduction-related volcanism.

*From*: Lucchi, F., Peccerillo, A., Keller, J., Tranne, C. A. & Rossi, P. L. (eds) 2013. *The Aeolian Islands Volcanoes*. Geological Society, London, Memoirs, **37**, 491–510. http://dx.doi.org/10.1144/M37.15 

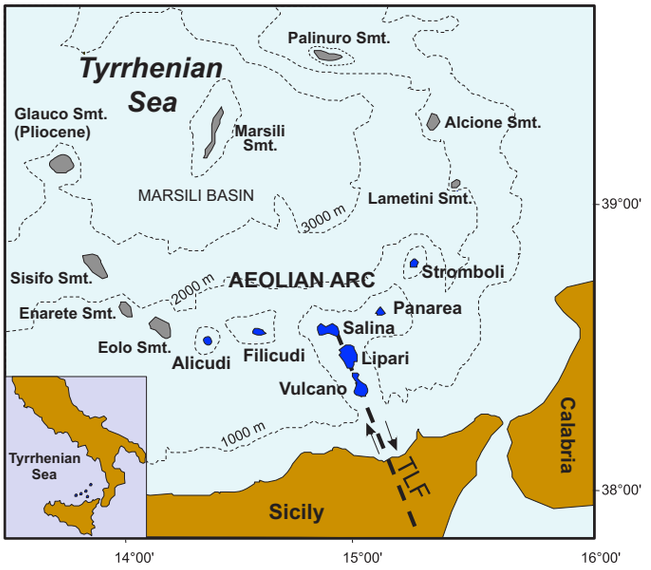


**Fig. 15.1.** Location map of Aeolian islands and seamounts. TLF is the Tindari–Letojanni Fault system.

## *Stuctural and volcanological setting*

The Aeolian volcanoes are composite structures formed by the superposition of multiple centres and recurrent volcanic and tectonic events, with many sector and central collapses. Rocks exposed above the sea level are younger than *c.* 270 ka (Gillot 1987; Leocat 2011). Vulcano and Stromboli are presently active, but Lipari and Panarea have also erupted or demonstrated intense submarine degassing during historical time. Of the seamounts, Marsili and Palinuro are considered active. Marsili rises for more than 3000 m over the sea floor of the Marsili basin, and is the best studied among Aeolian seamounts (Trua *et al.* 2011).

The Aeolian islands are constructed upon the Calabro–Peloritano basement, a block of the European continent which detached from Sardinia–Corsica and migrated south-westwards during the Miocene–Quaternary opening of the Tyrrhenian Sea. Crustal thickness beneath the Aeolian arc is *c.* 15–25 km, and increases westwards. The Aeolian arc is cut by a complex pattern of fault systems (Ventura 2013). The NW–SE-trending Tindari–Letojanni Fault (TLF) is the most important tectonic lineament in the area, running from the Salina–Lipari–Vulcano alignment to the Malta escarpment (Fig. 15.1). In mainland Sicily, the TLF cuts the Calabro–Peloritano basement near the boundary with the post-Miocene accretionary prism and the Iblei continental block to the west (Grasso 2001). It is likely that these geometric relationships continue in the Aeolian arc. This implies that distinct types of basement rocks are present across the Aeolian archipelago, that is, the Calabro–Peloritano basement in the central-eastern sectors and the accretionary prism rocks under the western islands. Such a hypothesis is supported by the increase in crustal thickness west of the Tindari–Letojanni Fault (Ventura 2013).

Traditionally, the Aeolian arc has been divided into three main sectors – the western, the central and the eastern arcs – which are characterized by first-order volcanological, magmatic and structural differences (Peccerillo 2005; Ventura 2013). The western arc is formed by Alicudi and Filicudi, which are situated along east–west- to WNW–ESE-striking fault systems. A NNW–SSE compressive strain field due to the Africa–Eurasia convergence is active in this sector (Ventura 2013). The central islands of Vulcano and Lipari are located along the TLF, where a strike-slip strain regime is active. Salina is sited at the intersection between the east–west-trending structures of the western arc and the Tindari–Letojanni Fault. Panarea and Stromboli are situated along SW–NE-trending faults. An extensional tectonic regime affects this sector of the arc.

Active volcanism occurs along the Tindari–Letojanni Fault and east of this tectonic line. The compressive tectonic regime in the western sector inhibits upraise and eruption of magmas, whereas extensional and strike-slip strain regimes in the central-eastern arc generate vertical faults that are pathways along which magmas ascend and erupt at the surface (Ventura 2013).

Geophysical studies (e.g. Panza *et al.* 2003) indicate that deep seismicity (up to 550 km) only occurs east of the Tindari–Letojanni Fault. This is a consequence of the Ionian slab subduction beneath the Calabro–Peloritano basement and the southern Tyrrhenian Sea. Active Aeolian volcanism is therefore located above or at the margin of the deep seismicity zone.

## *Magma compositions*

Key geochemical data from the literature are shown in Figures 15.2–15.6. The important information contained in these diagrams can be summarized as follows.

(1) Calc-alkaline (CA) and high-K calc-alkaline (HKCA) rocks occur throughout the arc but dominate at Alicudi, Filicudi, Salina, Lipari and Panarea (Fig. 15.2). In contrast, shoshonites (SHO) are spatially restricted to the central-eastern islands, where they generally appear during the mature to late stage of volcanic activity. The Marsili seamount has a CA basalt to basaltic andesite composition, with a few andesites (Trua *et al.* 2011). A single sample has ocean-island basalt (OIB)-type affinity and is not plotted in the diagrams. The small number of analyses available for the other Aeolian seamounts (not shown) indicates that rocks are predominantly of calc-alkaline mafic to intermediate composition, with a few shoshonites (Eolo, Enarete) and arc tholeiites (Marsili basin margin; Trua *et al.* 2004; Peccerillo 2005).

(2) The degree of magma evolution increases from the external to the central islands; rhyolitic volcanism ($SiO_2$ >70%) is present at Panarea and Salina, and becomes abundant at Lipari and Vulcano (Fig. 15.2). Rhyolites characterize the younger stages of activity for all these volcanoes.

(3) Abundances of elements that are incompatible with main magmatic minerals (e.g. Th, U, Nb, Ta and Light Rare Earth Elements - LREE) increase with silica for all the islands and seamounts (Fig. 15.3). The exception observed is for Ba, which decreases in the rhyolites of Vulcano and Lipari, but not in the rhyolites of Salina and Panarea (Fig. 15.3d).

(4) Incompatible trace element (ITE) abundances increase from CA to SHO volcanics for the mafic-intermediate compositions (Fig. 15.4). This is observed for both the large-ion lithophile elements (LILE: Rb, Ba, La, Th, etc.) and for the high-field-strength elements (HFSE: Nb, Ta, Hf, Zr). However, there are several differences between islands. These have important petrogenetic implications, and will be discussed later (see "Isotope and trace element composition of mantle sources").

(5) Incompatible element patterns normalized to primordial mantle for basalts and basaltic andesites from the Aeolian islands and Marsili seamount display the typical features of arc volcanics worldwide, with enrichments in LILE and relative depletion in HFSE (Fig. 15.5). Most of these features are also shown by the Calabro–Peloritano basement and the Ionian Sea sediments (Fig. 15.5d). The Aeolian seamounts (not shown) show similar patterns as the other Aeolian rocks, with fractionation and abundances of ITE increasing from CA to SHO rocks.

(6) Sr-isotope ratios of mafic–intermediate rocks increase from the western island of Alicudi to the central and eastern islands, reaching maximum values at Stromboli (Fig. 15.6a). Sr–Nd isotopic ratios display the well-known

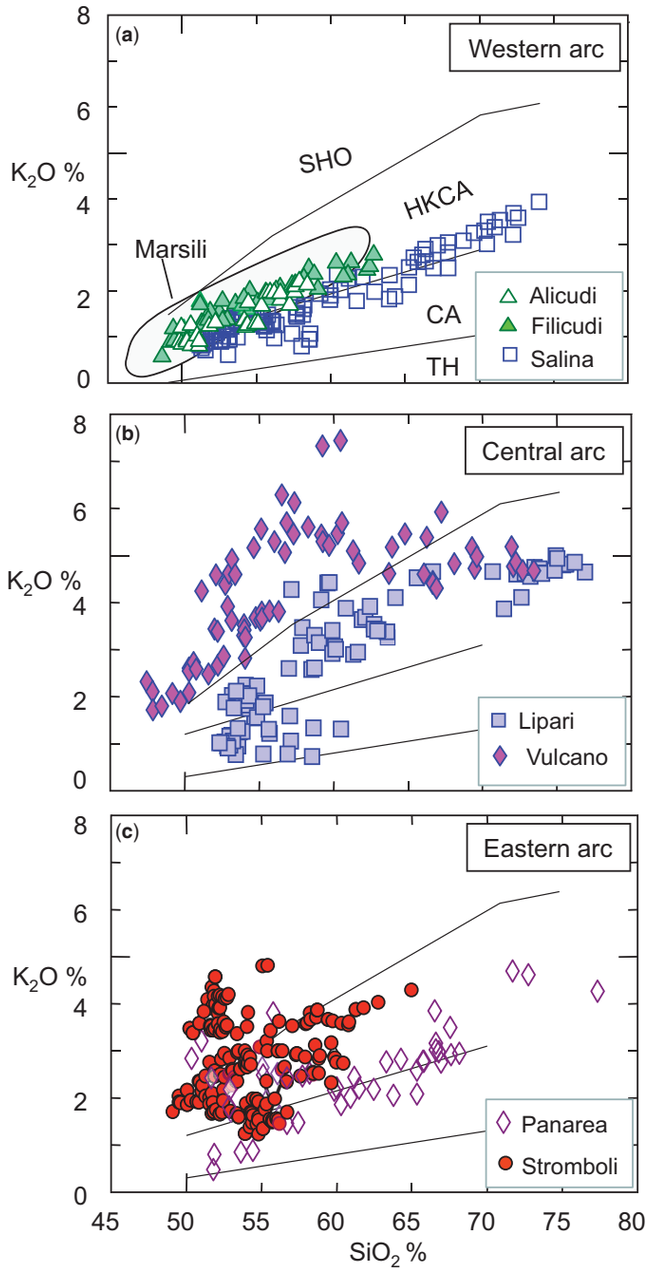


**Fig. 15.2.** $K_2O$ v. $SiO_2$ classification diagrams for the Aeolian arc volcanics. Lines dividing arc tholeiitic (TH), calc-alkaline (CA), high-K calc-alkaline (HKCA) and shoshonitic (SHO) series are from Peccerillo & Taylor (1976). Data on Marsili are from Trua *et al.* (2011). For source of other data see Peccerillo (2005).

negative correlation. However, a slightly steeper slope characterizes the western-central islands. Marsili shows a large Sr–Nd isotope variation that overlaps the western-central arc domain. Panarea has a variable Sr-Nd isotopic composition, with CA rocks falling within the field of western islands and SHO rocks plotting with Stromboli. At Stromboli there is a considerable increase of Sr- and a concomitant decrease of Nd-isotopic ratios from calc-alkaline to shoshonitic rocks (Francalanci *et al.* 1988, 1989, 2013), which is not observed at Vulcano (De Astis *et al.* 2000). Normalized $^3He/^4He$ ($R/R_a$) ratios (not shown) range from 7.07 (Alicudi) to 2.51 (Stromboli) (Martelli *et al.* 2008).

(7) Pb-isotope ratios have variable and overlapping values for most islands except for Stromboli, which has a distinctively less radiogenic Pb-isotope composition. Overall, Pb-isotope ratios fall between the highly radiogenic Etna OIB-type basalts and the continental crust of the Calabro–Peloritano basement (Fig. 15.6b). Etna is close to the so-called FOZO (=FOcus ZOne; Hart *et al.* 1992) mantle composition, which is extremely common in anorogenic settings of Europe and has been termed the European Asthenospheric Reservoir (EAR) by Wilson & Downes (1991). The Pb-isotope composition of Marsili overlaps Stromboli and some of the western-central islands.

(8) Stromboli shows similar radiogenic isotope signatures as Vesuvio (De Astis *et al.* 2000, 2013; Peccerillo 2001) and other volcanoes from Campania. Such a similarity is also observed for several incompatible trace element ratios, and led Peccerillo (2001) to conclude that Vesuvio and other Campania volcanoes represent the northern end of the Aeolian arc rather than the southern sector of the Roman Magmatic Province, as generally acknowledged.

## Shallow-level magma evolution

Fractional crystallization, crustal assimilation, magma mixing or some combination of these processes has been documented for the Aeolian volcanoes. These have been extensively discussed within individual chapters of this volume, so are only summarized briefly here.

### *Fractional crystallization*

Fractional crystallization was the predominant process of magma evolution at several centres. This process was much more intense for the volcanoes of the central islands, where rhyolitic compositions were reached. This outcome is likely related to local tectonics associated with the Tindari–Letojanni transcurrent fault, where the development of pull-apart basins favoured the formation of large reservoirs (Barberi *et al.* 1994) in which magmas ponded and fractionated. Mafic minerals plus plagioclase were main fractionating phases, as demonstrated by curvilinear trends for many major and trace elements, especially MgO, Ni, Cr but also $Al_2O_3$ and Sr, against $SiO_2$ (Fig. 15.3). A decrease of Ba in the rhyolites of Vulcano and Lipari, but not at Panarea and Salina, indicates significant separation of alkali-feldspar late in the evolution stages of the two former islands. Alkali-feldspar crystallization is related to the HKCA to SHO affinity of late erupted magmas at Lipari and Vulcano. Fractional crystallization modifies major and trace element abundances of magmas, slightly modifies $\delta^{18}O‰$, but leaves radiogenic isotope compositions and incompatible trace element ratios unaffected. The values of these parameters measured in evolved rocks can therefore be used to infer compositions of primary melts and their mantle sources. However, the main problem is that magma evolution rarely (if ever) occurs simply by closed-system fractional crystallization; wall-rock assimilation and magma mixing usually accompany fractional crystallization in most cases.

### *Magma mixing/mingling*

Magma mixing/mingling is widespread in the Aeolian volcanoes. The most striking evidence of this process is seen in the occurrence of abundant mafic enclaves in many intermediate and silicic lavas. These enclaves are blobs of mafic magmas that were present within the volcanic system and were intermingled with the silicic melts during eruption. The best examples are observed for some Lipari and Vulcano rhyolites (e.g. De Rosa & Sheridan 1983; Gioncada *et al.* 2005; Perugini *et al.* 2007; De Astis *et al.* 2013; Forni *et al.* 2013), for Panarea dacites and rhyolites (Calanchi *et al.*

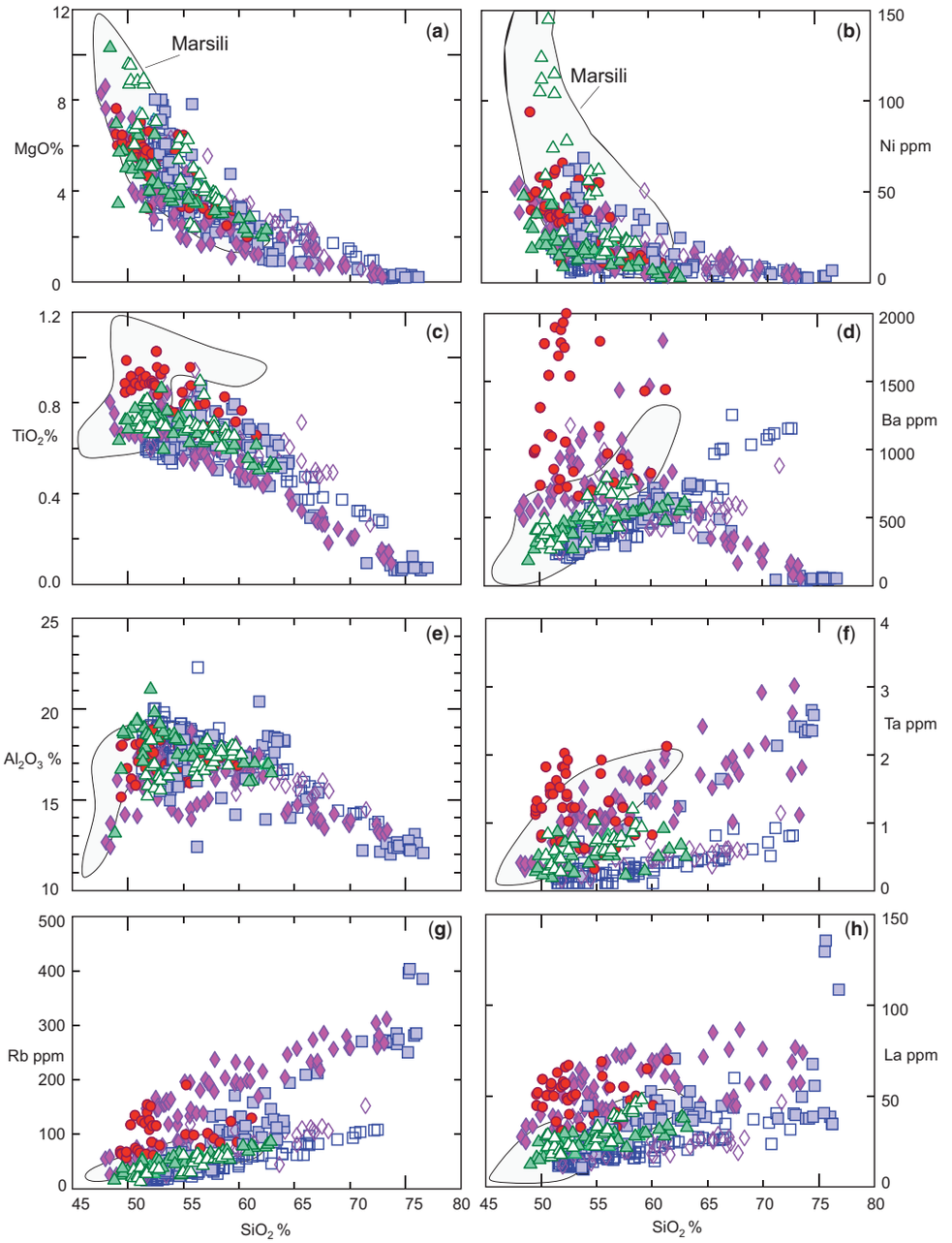


**Fig. 15.3.** Variation diagrams of some major and trace elements v. silica. Source of data and symbols as in Figure 15.2.

2002; Lucchi *et al.* 2013*d*) and at Salina (Perugini *et al.* 2004; Lucchi *et al.* 2013*c*). Mixing processes also affected most (if not all) of the magmas however, although physical evidence is less strong either because of the lack of compositional contrast between end-members or because near-equilibrium conditions were reached by hybrid magmas.

Mixing is a complex process of major geochemical and volcanological interest. Detailed studies in the Aeolian arc are however limited (e.g. De Rosa & Sheridan 1983; De Astis *et al.* 1997; Gioncada *et al.* 2003, 2005; Perugini *et al.* 2004, 2007; Davì *et al.* 2008; Piochi *et al.* 2009), and the effects on magma compositions for single eruptions, for individual volcanic centres and at the regional scale, are still basically unexplored.

### *Magma contamination*

Magma contamination by crustal wall-rocks in the Aeolian volcanoes took place as a consequence of several different processes. Assimilation plus fractional crystallization (AFC) is the most common case, and has been recognized at several islands (e.g. Salina, Vulcano and Lipari; Crisci *et al.* 1991; Esperança *et al.* 1992; De Astis *et al.* 2013; Forni *et al.* 2013; Lucchi *et al.* 2013*c*). This is clearly demonstrated by the positive correlations of $^{87}Sr/^{86}Sr$ and $\delta^{18}O‰$ with silica observed for many Aeolian islands by Ellam & Harmon (1990). More complex processes of combined fractional crystallization, assimilation, refilling of magma chambers, mixing and frequent tapping by eruptions (RFTA: refilling, fractionation, tapping, assimilation) have been recognized for the lowest exposed volcanic sequences of many islands (e.g. De Astis *et al.* 1997; Di Martino *et al.* 2011; Lucchi *et al.* 2013*a*, *b*, c). These rocks are generally mafic in composition and display rather variable trace element and isotopic signatures, which is typical of RFTA processes (O'Hara 1977). Finally, a particular type of assimilation is represented by incorporation of different amounts of crustal rocks by basaltic and andesitic magmas, with the former being able to assimilate greater amounts of crustal rocks than andesites. Such a process has been

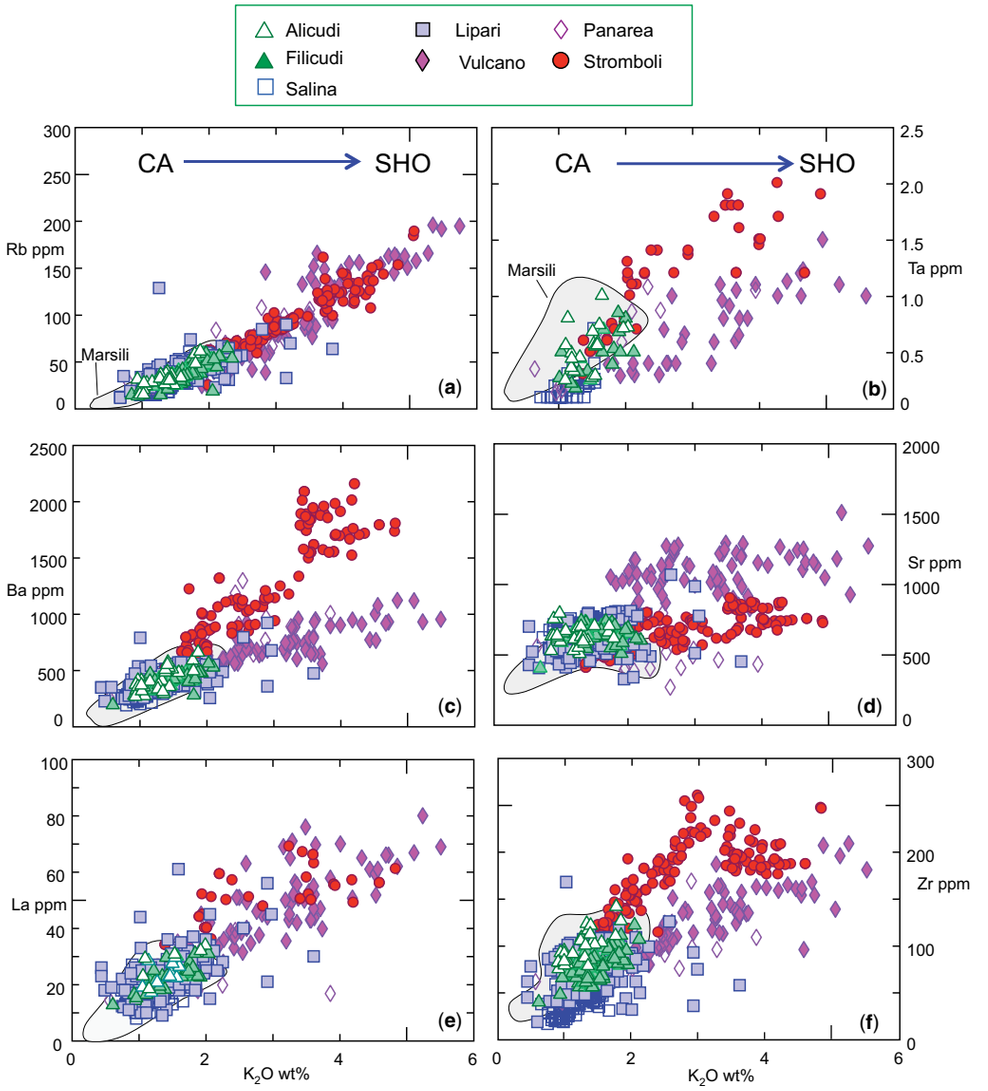


**Fig. 15.4.** Incompatible trace element v. $K_2O$ diagrams for mafic-intermediate rocks ($SiO_2$ <56 wt%) from the Aeolian arc and Marsili seamount, showing increase of element abundances from calc-alkalic to shoshonitic rocks. Source of data as in Figure 15.2.

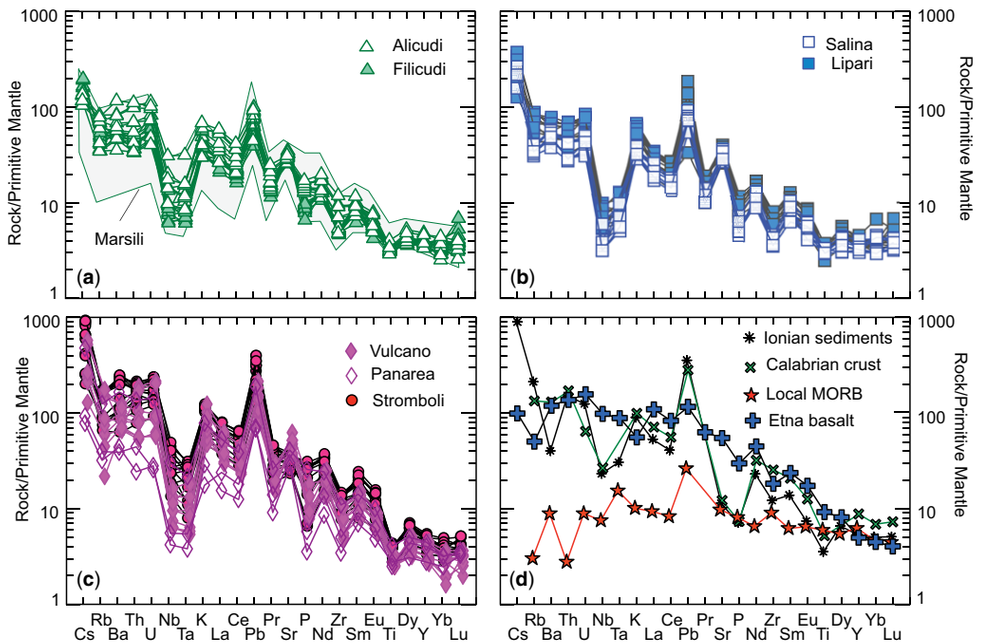


**Fig. 15.5.** Incompatible element patterns normalized to primordial mantle compositions for representative mafic-intermediate rocks ($SiO_2$ <56 wt%) from the Aeolian islands and Marsili seamount (source of data as in Fig. 15.2). Ionian sediments (average of two samples; De Astis, unpublished data), averages of the Calabro–Peloritano basement (Rottura *et al.* 1991), Tyrrhenian MORB (Dietrich *et al.* 1977) and Etna basalts (Viccaro & Cristofolini 2008) are also shown. Normalizing data are from Sun & McDonough (1989).

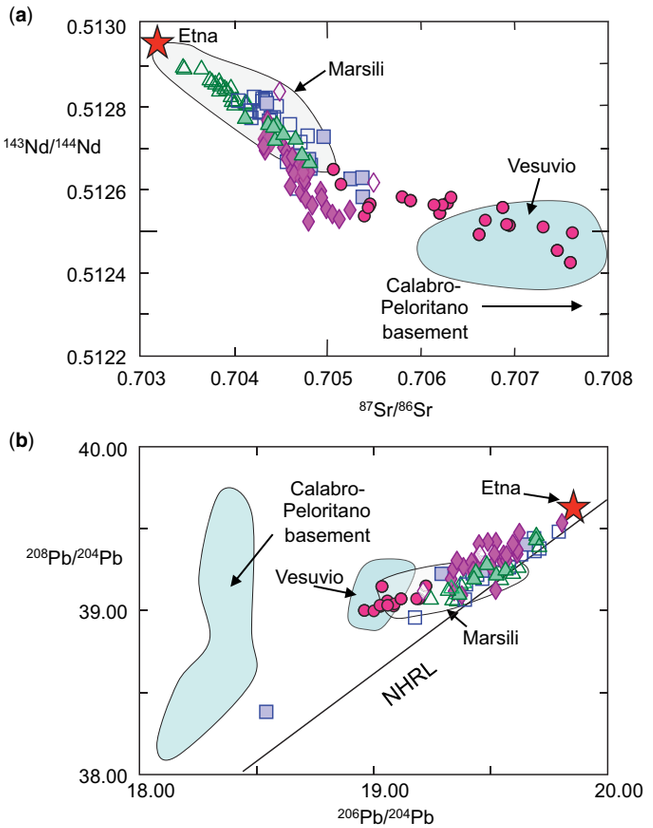


**Fig. 15.6.** Sr–Nd–Pb isotopic compositions for mafic-intermediate rocks ($SiO_2 < 56\%$) from the Aeolian arc and Marsili seamount. Source of data and symbols as in Figures 15.2 and 15.4. Alicudi and Filicudi andesites ($SiO_2 = 56–62\%$) are also plotted, since these represent the least-contaminated magmas in the Aeolian arc (see text). Average Etna basalts (Viccaro & Cristofolini 2008) and compositions fields of Vesuvio (for source of data see Peccerillo 2005) and Calabro–Peloritano basement (Rottura *et al.*, 1991) are also reported. NHRL (Northern Hemisphere Reference Line) is from Hart (1984).

well documented at Alicudi, where evolved andesites were less affected by assimilation and, consequently, exhibit more primitive isotopic compositions (i.e. lower Sr- and O- and higher Nd–Pb isotope ratios) than associated basalts (Peccerillo & Wu 1992; Peccerillo *et al.* 1993; Lucchi *et al.* 2013*a*). The same process has been recognized, although less clearly, at Filicudi (Santo & Peccerillo 2008; Lucchi *et al.* 2013*b*).

Several studies on Aeolian volcanoes demonstrated that magma–wall-rock interaction produced an increase in both $^{87}Sr/^{86}Sr$ and $\delta^{18}O‰$ (Ellam & Harmon 1990; Peccerillo *et al.* 2004; Santo & Peccerillo 2008). However, whereas O-isotope ratios were increased from typical mantle values of $\delta^{18}O‰$ *c.* +5.5 to values as high as $\delta^{18}O‰$ *c.* +8.5, Sr isotope ratios were less strongly modified. Detailed studies of two contaminated suites of mafic magmas from Alicudi and Vulcano (Primordial Vulcano and Piano Caldera) have shown that extensive crustal assimilation generated an increase in Sr isotope ratios by five to six digits on the fourth decimal place (De Astis *et al.* 1997, 2013; Lucchi *et al.* 2013*a*). This is one order of magnitude lower than the variation observed over the Aeolian arc. Some incompatible element ratios, such as Rb/Ba, Rb/Sr and Ba/K, are significantly correlated with Sr-isotope variation, suggesting they were modified by contamination. By contrast, other element ratios such as Ba/La, Rb/Nb, U/Th, Sr/Nd and Tb/Yb do not show any correlation with Sr isotope ratios, implying that they were less affected or unaffected by contamination. Such different behaviour is related to the variable compositional contrast between magma and wall rocks for various elements. This changes from one volcanic centre to another however, and results found at Alicudi and Vulcano cannot be considered as valid for the entire Aeolian arc.

## Conditions of magma ponding and ascent

Conditions of magma ponding, crystallization and ascent have been examined using two different approaches. One is based on measurements of crystallographic parameters of clinopyroxenes, especially cell dimensions, under the assumption that these depend on pressure of crystallization (e.g. Nazzareni *et al.* 1998, 2001). Other work has focused on fluid inclusions in quartz-rich xenoliths (Frezzotti *et al.* 2003, 2004; Zanon *et al.* 2003; Frezzotti & Peccerillo 2004; Peccerillo *et al.* 2006; Di Martino *et al.* 2010, 2011).

Clinopyroxene studies have documented crystallization at different pressures within the volcanic systems, suggesting the occurrence of various depths of magma storage and fractionation at the regional scale. Fluid inclusion studies provided additional insight into magma evolution, confirming polybaric mineral crystallization and demonstrating that mafic to intermediate magmas ponded in deep reservoirs sited at depths of 21–18 km in the lower crust at the mantle-crust boundary. Here, magmas were subjected to fractionation and assimilation processes, plus intensive feeding by mantle-derived mafic melts (RFTA). At Lipari, long-lived hot mafic magma reservoirs facilitated partial melting of the lower continental crust, as testified by the eruption of cordierite-, garnet-, and sillimanite-bearing lavas (Barker 1987; Di Martino *et al.* 2011). By contrast, dacitic and rhyolitic magmas were generated by dominant fractional crystallization of mafic parental magmas in reservoirs located at depths of 15–12 km. Since felsic magmas are restricted to the younger stages of activity at many Aeolian volcanoes, an overall upward migration of the magma chambers with time has been suggested (Peccerillo *et al.* 2006). The reasons for such a migration are still poorly understood. A variation of local tectonic stress may have allowed formation of mid-crustal reservoirs (Ventura 2013). Another possibility could be that there was a decrease in the input of mafic magmas into the deep reservoirs during the mature to latest (and vanishing?) stages of volcanism. This would have allowed fractional crystallization to become dominant with respect to input and mixing with fresh mafic magmas, favouring the formation of evolved melts. These were able to rise more readily than mafic magmas to shallow crustal levels because of their lower density.

## Mantle source composition, magma genesis and geodynamic setting

Trace element and isotope data are crucial for understanding the composition and evolution of mantle sources and for exploring conditions of magma genesis and geodynamic evolution. Many geochemical studies have therefore been carried out on the Aeolian volcanoes. Much attention has been focused on mafic magmas, under the assumption that they represent primary compositions. However, such a statement has been proven incorrect for some mafic magma suites such as at Alicudi and Filicudi. The possible effects of magma contamination have to be considered before inferring compositions of primary melts and their mantle sources.

### *Isotope and trace element composition of mantle sources*

Regional variations of radiogenic isotope ratios for mafic rocks in the Aeolian arc have long been recognized and attributed to

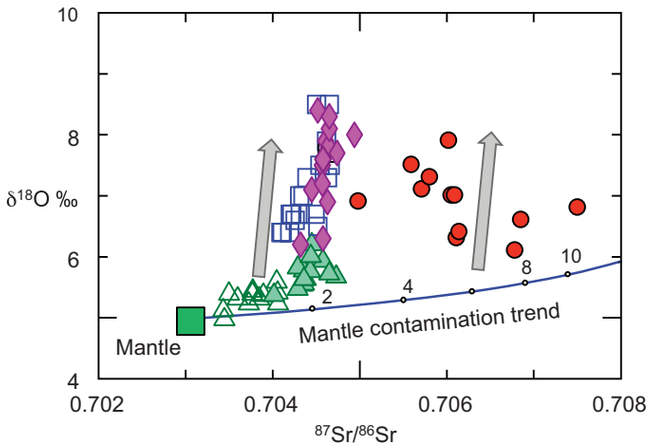


**Fig. 15.7.** $\delta^{18}O$ v. $^{87}Sr/^{86}Sr$ for Aeolian magmas. The solid line represents the mixing trend between primordial mantle and Ionian sediments (mantle contamination). Numbers along the line are the amounts of sediments involved in the mixing. Arrows mimic effects of magma contamination by crustal wall rocks: note strong oxygen isotope variation and modest increase of Sr isotope ratios. Data for Filicudi, Alicudi and Vulcano have been determined on separated clinopyroxene phenocrysts (Peccerillo *et al.* 2004; Santo & Peccerillo 2008; De Astis, unpublished data) and melt compositions have been calculated considering high-temperature isotope fractionations. Data on the other islands are bulk rock determinations (Ellam & Harmon 1990; Gertisser & Keller 2000). Symbols as in Figure 15.4.

heterogeneities of the mantle wedge (e.g. Ellam *et al.* 1988; Ellam & Harmon 1990; Francalanci *et al.* 1993; De Astis *et al.* 2000; Peccerillo *et al.* 2004). However, the common occurrence of magma–crust interaction raises the problem of how much of this variation is due to magma contamination and how much to source heterogeneity.

Combined O- and Sr-isotope studies can help to discriminate magma contamination from source contamination processes. Figure 15.7 represents a $\delta^{18}O‰$ and $^{87}Sr/^{86}Sr$ diagram for the available data on Aeolian rocks and separated phases (Ellam & Harmon 1990; Peccerillo *et al.* 2004; Santo & Peccerillo 2008; De Astis, unpublished data). The solid line describes a model of bulk mixing between a primordial mantle source and Ionian Sea sediments. Only a small number of samples from Alicudi and a few from Filicudi plot on or just above the mantle–sediment mixing line. By contrast, most of the Filicudi samples are shifted upwards and show high $\delta^{18}O‰$, which is typical of contaminated magmas. Well-defined vertical trends are shown by Salina and Vulcano samples, whereas Stromboli shows scattering and plots away from the mantle–sediment mixing line.

Although the above model has to be considered as broadly qualitative because of the simplistic assumptions of simple bulk mixing and uniform compositions for end-members, O–Sr isotope data indicate that a few of the Alicudi and Filicudi magmas can be considered as near-primary in composition. Their different Sr-isotope signatures at the same $\delta^{18}O‰$ value suggest less radiogenic Sr compositions for Alicudi magmas and their sources. The vertical data arrays for Vulcano and Salina highlight strong variation of $\delta^{18}O$ with a modest increase of $^{87}Sr/^{86}Sr$, typical of magma contamination (Ellam & Harmon 1990). However, if these trends are extrapolated back to the mantle–sediment mixing line, Sr-isotope ratios similar to those at Filicudi are deduced (i.e. $^{87}Sr/^{86}Sr$ slightly higher than 0.704). Stromboli does not show typical magma contamination trends but no samples fall on the mantle–sediment mixing line, suggesting that the Stromboli magmas are also contaminated but that Sr-isotope compositions are more variable and radiogenic than at other islands.

To summarize, the O–Sr isotope data suggest that there are few uncontaminated magmas in the Aeolian arc. Magma contamination processes had minor effects on Sr isotope ratios however, in agreement with studies on Alicudi and Primordial Vulcano discussed previously (see "Shallow-level magma evolution"). This leads to the conclusion that first-order Sr-isotope variation along the Aeolian arc is a direct manifestation of source heterogeneity. The same can be demonstrated for other radiogenic isotopes.

Variations of Sr–Pb isotope ratios along the arc are shown in Figure 15.8, to better highlight regional isotopic zoning. There is an increase of the $^{87}Sr/^{86}Sr$ ratio from Alicudi to Filicudi and the central islands, where the lowest Sr-isotope values are slightly above 0.704. Another increase in radiogenic Sr is observed at Stromboli. Nd isotopic compositions exhibit a similar trend, although anti-corrrelated with Sr-isotope variations. Ranges of Pb-isotope ratios remain fairly constant across most of the arc, but become less radiogenic at Stromboli. The back-arc Marsili seamount has a rather wide range of Sr–Nd isotope compositions, comparable to those observed over the entire western arc. A very low $^{206}Pb/^{204}Pb$ is observed for one sample from Lipari (Esperança *et al.* 1992).

Trace element abundances and ratios provide additional information on mantle composition. Here, this issue is examined by using a new set of trace element data (Table 15.1) for more than 90 mafic–intermediate rocks from different stratigraphic levels on various islands. The new data have the advantage of minimizing the inter-laboratory analytical bias that characterizes the data in the literature, thus providing a confident picture of geochemical zoning along the arc. Inferences on source composition are based on trace element contents of both mafic and intermediate rocks, since andesitic rocks at Alicudi have been shown to represent the least contaminated magmas across the entire arc (Peccerillo *et al.* 1993; Lucchi *et al.* 2013*a*). Moreover, only trace element ratios that have not shown systematic variation with Sr-isotope ratios in the contaminated mafic rocks of Vulcano and Alicudi are considered, under the assumption that they may provide reliable information on mantle compositions. The

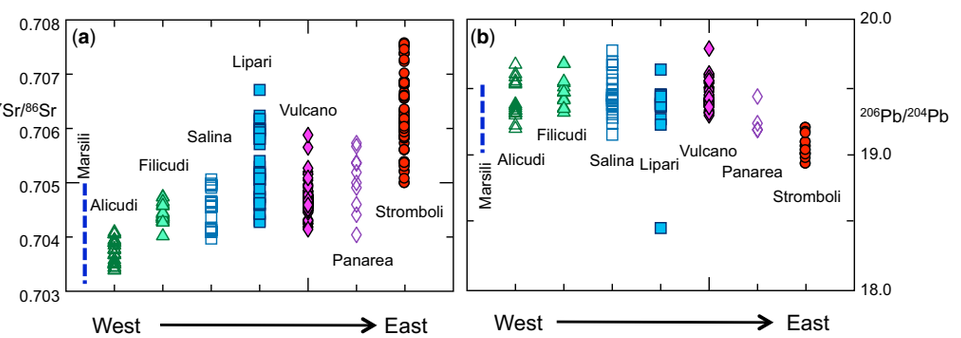


**Fig. 15.8.** Regional variation of Sr–Pb isotopic compositions for mafic-intermediate rocks ($SiO_2$ <56 wt%) from the Aeolian arc. Alicudi and Filicudi andesites ($SiO_2$ = 56–62%) are also plotted, since these represent the least contaminated magmas in the Aeolian arc (see text). Data of Marsili seamount are shown as a dashed line on the left-hand side of the diagrams. Source of data as in Figure 15.2.

**Table 15.1.** *Major and trace element data for representative rocks from Aeolian volcanoes. Major element data for Vulcano and Panarea are from De Astis* et al. *(1997) and Calanchi* et al. *(2002)*

| Sample | A9 ALI Alicudi | A3 ALI Alicudi | A6 ALI Alicudi | A11 ALI Alicudi | A15 ALI Alicudi | A4 ALI Alicudi | A7 ALI Alicudi | A5 ALI Alicudi | FIL 95 Filicudi | FIL 90 Filicudi | FIL 9 Filicudi | FIL10 Filicudi | FIL 7 Filicudi | FIL 80 Filicudi | FIL101 Filicudi |
|---|---|---|---|---|---|---|---|---|---|---|---|---|---|---|---|
| $SiO_2$ | 51.10 | 51.42 | 54.03 | 55.07 | 56.27 | 56.32 | 56.99 | 58.84 | 48.78 | 50.20 | 50.58 | 50.62 | 50.96 | 50.99 | 51.43 |
| $TiO_2$ | 0.69 | 0.72 | 0.77 | 0.69 | 0.92 | 0.72 | 0.66 | 0.77 | 0.72 | 0.75 | 0.77 | 0.77 | 0.72 | 0.83 | 0.81 |
| $Al_2O_3$ | 16.93 | 16.98 | 17.84 | 16.49 | 18.94 | 18.68 | 18.35 | 18.86 | 18.92 | 18.65 | 18.47 | 19.44 | 18.05 | 19.30 | 18.78 |
| $Fe_2O_3$ | 3.96 | 7.71 | 1.96 | 3.24 | 3.31 | 2.12 | 2.27 | 4.71 | 9.40 | 9.84 | 9.06 | 8.88 | 8.73 | 9.91 | 9.61 |
| FeO | 3.82 | 0.87 | 5.26 | 3.74 | 3.30 | 4.19 | 3.79 | 0.98 | 0.00 | 0.00 | 0.00 | 0.00 | 0.00 | 0.00 | 0.00 |
| MnO | 0.09 | 0.10 | 0.09 | 0.09 | 0.09 | 0.09 | 0.09 | 0.07 | 0.16 | 0.17 | 0.16 | 0.16 | 0.16 | 0.16 | 0.16 |
| MgO | 8.20 | 7.16 | 6.05 | 6.49 | 2.43 | 4.00 | 4.48 | 2.23 | 5.70 | 4.92 | 3.54 | 3.44 | 4.73 | 3.93 | 3.94 |
| CaO | 10.45 | 10.36 | 8.61 | 8.71 | 7.56 | 7.43 | 7.10 | 5.73 | 11.44 | 11.00 | 11.00 | 10.67 | 10.20 | 9.77 | 10.48 |
| $Na_2O$ | 2.52 | 2.25 | 3.24 | 3.18 | 3.78 | 3.50 | 3.72 | 4.20 | 2.28 | 2.39 | 2.72 | 2.69 | 2.75 | 2.65 | 2.68 |
| $K_2O$ | 0.95 | 0.94 | 1.55 | 1.27 | 1.75 | 1.82 | 1.90 | 2.15 | 1.16 | 1.01 | 1.01 | 1.17 | 1.28 | 1.27 | 1.37 |
| $P_2O_5$ | 0.29 | 0.30 | 0.33 | 0.32 | 0.37 | 0.34 | 0.36 | 0.39 | 0.22 | 0.20 | 0.19 | 0.18 | 0.21 | 0.20 | 0.23 |
| LOI | 0.99 | 1.19 | 0.27 | 0.71 | 1.28 | 0.79 | 0.29 | 1.07 | 1.23 | 0.87 | 2.51 | 1.99 | 2.22 | 1.00 | 0.52 |
| V | 223 | 221 | 221 | 223 | 169 | 180 | 163 | 137 | 330 | 240 | 308 | 290 | 285 | 271 | 331 |
| Ga | 13 | 14 | 16 | 15 | 16 | 16 | 13 | 16 | 19 | 19 | 17 | 20 | 17 | 21 | 17 |
| Rb | 24 | 23 | 40 | 28 | 48 | 55 | 47 | 52 | 23 | 27 | 23 | 34 | 34 | 32 | 30 |
| Sr | 583 | 606 | 598 | 570 | 623 | 667 | 642 | 686 | 679 | 729 | 708 | 763 | 723 | 773 | 713 |
| Y | 17 | 17 | 18 | 16 | 23 | 19 | 18 | 22 | 17 | 18 | 17 | 18 | 18 | 19 | 18 |
| Zr | 63 | 56 | 83 | 83 | 107 | 112 | 107 | 139 | 54 | 60 | 56 | 63 | 63 | 59 | 55 |
| Nb | 7.4 | 7.3 | 10.6 | 11.0 | 10.6 | 14.9 | 13.1 | 23.1 | 4.8 | 5.8 | 5.6 | 7.0 | 6.9 | 6.0 | 4.6 |
| Cs | | 0.95 | | | 1.09 | 1.12 | 0.86 | 0.97 | | 1.32 | 1.37 | 1.58 | | | 1.18 |
| Ba | 343 | 260 | 417 | 499 | 453 | 607 | 593 | 852 | 335 | 402 | 373 | 406 | 410 | 382 | 379 |
| La | 21 | 19 | 25 | 27 | 30 | 40 | 38 | 42 | 15 | 20 | 16 | 20 | 20 | 19 | 19 |
| Ce | 40 | 38 | 46 | 49 | 56 | 69 | 67 | 77 | 30 | 37 | 33 | 43 | 41 | 39 | 36 |
| Pr | 4.0 | 4.2 | 4.6 | 4.7 | 5.5 | 6.4 | 6.1 | 7.2 | 3.3 | 4.1 | 3.7 | 4.7 | 4.4 | 4.4 | 4.0 |
| Nd | 16 | 18 | 20 | 19 | 24 | 26 | 24 | 28 | 16 | 18 | 15 | 19 | 19 | 19 | 18 |
| Sm | 3.50 | 3.54 | 3.37 | 3.74 | 4.51 | 4.26 | 4.28 | 5.43 | 4.18 | 4.57 | 4.24 | 3.97 | 4.42 | 3.89 | 4.12 |
| Eu | 1.06 | 0.95 | 1.16 | 1.11 | 0.91 | 1.32 | 0.87 | 1.01 | 1.06 | 1.01 | 1.33 | 1.31 | 1.14 | 0.74 | 1.14 |
| Gd | 3.44 | 4.11 | 3.53 | 2.74 | 4.10 | 3.43 | 3.48 | 4.35 | 2.87 | 4.77 | 3.89 | 3.42 | 3.91 | 4.24 | 2.12 |
| Tb | 0.49 | 0.50 | 0.53 | 0.43 | 0.62 | 0.59 | 0.55 | 0.57 | 0.52 | 0.43 | 0.45 | 0.53 | 0.55 | 0.55 | 0.44 |
| Dy | 2.86 | 3.42 | 3.17 | 3.01 | 4.04 | 3.31 | 3.28 | 3.73 | 3.03 | 2.76 | 3.14 | 3.28 | 3.33 | 3.30 | 3.01 |
| Ho | 0.60 | 0.63 | 0.64 | 0.55 | 0.69 | 0.63 | 0.59 | 0.80 | 0.60 | 0.62 | 0.69 | 0.66 | 0.54 | 0.63 | 0.63 |
| Er | 1.70 | 1.78 | 1.83 | 1.54 | 2.43 | 1.80 | 1.83 | 2.29 | 1.62 | 1.80 | 1.71 | 1.75 | 1.96 | 1.91 | 1.50 |
| Tm | 0.23 | 0.26 | 0.25 | 0.26 | 0.36 | 0.28 | 0.28 | 0.32 | 0.36 | 0.34 | 0.37 | 0.24 | 0.25 | 0.40 | 0.26 |
| Yb | 1.48 | 1.53 | 1.79 | 1.30 | 2.08 | 1.92 | 1.47 | 2.28 | 1.93 | 2.16 | 1.68 | 1.73 | 2.11 | 1.92 | 1.61 |
| Lu | 0.24 | 0.28 | 0.20 | 0.29 | 0.27 | 0.25 | 0.28 | 0.31 | 0.30 | 0.41 | 0.35 | 0.30 | 0.29 | 0.53 | 0.27 |
| Hf | 1.64 | 1.34 | 1.87 | 1.57 | 2.26 | 2.26 | 2.30 | 2.99 | 1.87 | 1.76 | 1.24 | 1.45 | 1.40 | 1.67 | 1.28 |
| Ta | 0.44 | 0.36 | 0.48 | 0.50 | 0.65 | 0.65 | 0.67 | 1.34 | 0.28 | 0.26 | 0.34 | 0.37 | 0.35 | | 0.30 |
| Pb | 5.1 | 3.3 | 5.6 | 4.9 | 5.5 | 5.7 | 6.1 | 6.9 | 3.8 | 2.9 | 5.8 | 6.6 | 6.8 | 4.1 | 4.6 |
| Th | 3.78 | 3.02 | 4.88 | 6.14 | 6.18 | 9.12 | 8.77 | 9.88 | 2.97 | 3.70 | 3.22 | 4.07 | 4.20 | 3.72 | 3.87 |
| U | 1.07 | 0.89 | 1.56 | 1.81 | 1.61 | 2.49 | 2.12 | 2.24 | 0.99 | 1.20 | 1.01 | 1.44 | 1.80 | 1.17 | 1.19 |

| Sample | FIL 40 Filicudi | FIL 29 Filicudi | FIL 24 Filicudi | SAL 98a Salina | SAL 28 Salina | SAL 40 Salina | SAL 48 Salina | SAL 55 Salina | SAL 79 Salina | SAL 27 Salina | SAL 82 Salina | SAL 88 Salina | SAL 1 Salina | SAL 76 Salina | A1 LIP Lipari |
|---|---|---|---|---|---|---|---|---|---|---|---|---|---|---|---|
| $SiO_2$ | 52.38 | 52.68 | 53.28 | 49.50 | 49.53 | 49.79 | 50.02 | 50.76 | 50.93 | 51.03 | 51.46 | 51.81 | 52.03 | 52.15 | 52.17 |
| $TiO_2$ | 0.70 | 0.78 | 0.77 | 0.73 | 0.65 | 0.73 | 0.74 | 0.65 | 0.69 | 0.74 | 0.67 | 0.74 | 0.65 | 0.66 | 0.68 |
| $Al_2O_3$ | 19.56 | 18.17 | 17.00 | 17.84 | 19.13 | 17.87 | 19.77 | 17.85 | 20.09 | 19.32 | 18.53 | 17.50 | 18.07 | 17.36 | 17.30 |
| $Fe_2O_3$ | 8.87 | 9.66 | 8.30 | 11.44 | 9.82 | 11.56 | 11.31 | 10.15 | 9.83 | 10.62 | 9.91 | 10.95 | 9.63 | 9.88 | 9.58 |
| FeO | | 0.00 | 0.00 | 0.00 | 0.00 | 0.00 | 0.00 | 0.00 | 0.00 | 0.00 | 0.00 | 0.00 | 0.00 | 0.00 | 0.00 |
| MnO | 0.16 | 0.17 | 0.14 | 0.21 | 0.18 | 0.21 | 0.21 | 0.19 | 0.19 | 0.20 | 0.18 | 0.20 | 0.19 | 0.19 | 0.17 |
| MgO | 3.85 | 3.50 | 5.34 | 5.17 | 3.41 | 5.01 | 3.41 | 5.75 | 3.49 | 3.39 | 4.53 | 4.43 | 4.59 | 5.36 | 5.84 |
| CaO | 10.16 | 10.35 | 10.15 | 11.22 | 9.40 | 10.85 | 10.73 | 10.95 | 11.11 | 10.12 | 10.95 | 10.23 | 10.60 | 10.12 | 10.13 |
| $Na_2O$ | 2.82 | 2.51 | 2.65 | 2.39 | 2.47 | 2.29 | 2.58 | 2.31 | 2.68 | 2.78 | 2.36 | 2.38 | 2.34 | 2.42 | 2.22 |
| $K_2O$ | 1.28 | 1.20 | 1.55 | 0.96 | 0.75 | 0.99 | 0.97 | 0.92 | 0.84 | 0.91 | 0.88 | 1.08 | 1.18 | 0.98 | 1.14 |
| $P_2O_5$ | 0.22 | 0.15 | 0.34 | 0.11 | 0.12 | 0.10 | 0.10 | 0.12 | 0.12 | 0.12 | 0.11 | 0.16 | 0.11 | 0.14 | 0.15 |
| LOI | 0.00 | 0.82 | 0.49 | 0.45 | 4.52 | 0.60 | 0.16 | 0.35 | 0.04 | 0.76 | 0.42 | 0.54 | 0.62 | 0.74 | 0.63 |
| V | 291 | 298 | 263 | 304 | 328 | 309 | 310 | 285 | 380 | 266 | 286 | 299 | 294 | 309 | 239 |
| Ga | 21 | 20 | 16 | 15 | 19 | 14 | 18 | 16 | 17 | 15 | 17 | 16 | 16 | 18 | 15 |
| Rb | 33 | 36 | 45 | 22 | 20 | 23 | 19 | 20 | 21 | 20 | 21 | 26 | 26 | 22 | 38 |
| Sr | 656 | 737 | 561 | 717 | 716 | 771 | 762 | 576 | 730 | 770 | 699 | 709 | 732 | 609 | 602 |
| Y | 17 | 18 | 16 | 15 | 27 | 16 | 16 | 14 | 16 | 17 | 15 | 19 | 16 | 15 | 17 |
| Zr | 57 | 61 | 63 | 42 | 40 | 43 | 57 | 40 | 42 | 46 | 43 | 52 | 49 | 41 | 64 |
| Nb | 7.1 | 6.5 | 10.2 | 2.3 | 2.6 | 2.8 | 2.5 | 2.3 | 2.5 | 2.2 | 2.6 | 2.8 | 4.3 | 2.3 | 4.2 |
| Cs | | 1.63 | | | 1.21 | 1.26 | 1.54 | | | | | 2.13 | | 1.74 | 1.87 |
| Ba | 380 | 407 | 350 | 347 | 334 | 413 | 354 | 266 | 358 | 325 | 331 | 399 | 378 | 343 | 369 |
| La | 19 | 21 | 20 | 14 | 17 | 17 | 14 | 12 | 13 | 13 | 14 | 18 | 15 | 13 | 16 |
| Ce | 37 | 40 | 42 | 27 | 40 | 31 | 28 | 24 | 23 | 26 | 27 | 33 | 31 | 26 | 34 |
| Pr | 3.8 | 4.1 | 4.3 | 3.0 | 4.4 | 3.3 | 3.1 | 2.9 | 2.8 | 3.0 | 3.0 | 4.0 | 3.4 | 2.8 | 3.6 |
| Nd | 16 | 18 | 18 | 13 | 22 | 17 | 15 | 13 | 13 | 15 | 14 | 18 | 15 | 12 | 18 |
| Sm | 2.87 | 4.66 | 3.54 | 3.80 | 5.41 | 3.35 | 3.29 | 2.84 | 3.07 | 2.93 | 3.74 | 4.63 | 4.01 | 2.81 | 3.25 |
| Eu | 0.98 | 1.39 | 0.87 | 0.79 | 1.72 | 1.05 | 1.31 | 0.81 | 0.97 | 0.96 | 0.70 | 1.08 | 1.05 | 0.96 | 1.01 |
| Gd | 4.47 | 3.31 | 5.53 | 2.78 | 4.22 | 2.44 | 3.83 | 2.61 | 2.92 | 4.00 | 2.91 | 6.22 | 3.61 | 3.65 | 5.32 |
| Tb | 0.50 | 0.60 | 0.58 | 0.44 | 0.77 | 0.46 | 0.60 | 0.36 | 0.48 | 0.48 | 0.47 | 0.50 | 0.57 | 0.46 | 0.50 |
| Dy | 2.87 | 3.51 | 3.14 | 2.28 | 4.71 | 2.94 | 2.74 | 2.31 | 2.85 | 3.19 | 2.66 | 3.32 | 3.20 | 2.69 | 3.43 |
| Ho | 0.52 | 0.61 | 0.63 | 0.58 | 0.94 | 0.57 | 0.49 | 0.49 | 0.56 | 0.63 | 0.57 | 0.76 | 0.63 | 0.57 | 0.55 |
| Er | 1.70 | 2.03 | 1.73 | 1.24 | 2.78 | 1.61 | 1.60 | 1.56 | 1.60 | 1.44 | 1.40 | 1.65 | 1.50 | 1.33 | 1.54 |
| Tm | 0.28 | 0.28 | 0.30 | 0.31 | 0.45 | 0.29 | | 0.23 | 0.28 | 0.29 | 0.25 | | 0.32 | 0.36 | 0.37 |
| Yb | 2.10 | 1.85 | 1.50 | 2.12 | 2.76 | 2.28 | 1.60 | 1.51 | 1.27 | 1.75 | 1.55 | 2.12 | 2.17 | 1.48 | 1.89 |
| Lu | 0.25 | 0.30 | 0.32 | 0.30 | 0.37 | 0.30 | | 0.24 | 0.33 | 0.28 | 0.25 | | 0.32 | 0.29 | 0.39 |
| Hf | 1.76 | 1.58 | 1.48 | 1.29 | 1.18 | 0.93 | 1.09 | 0.89 | 0.95 | 1.48 | 0.86 | 1.68 | 1.50 | 1.14 | 1.45 |
| Ta | 0.30 | 0.34 | 0.52 | 0.21 | 0.13 | 0.23 | | | 0.21 | | 0.29 | | 0.40 | 0.23 | 0.27 |
| Pb | 7.4 | 5.9 | 4.7 | 5.8 | 5.7 | 6.6 | 6.2 | 3.9 | 4.5 | 4.0 | 5.6 | 5.8 | 5.5 | 5.2 | 7.4 |
| Th | 4.30 | 4.56 | 3.29 | 2.51 | 2.78 | 3.68 | 2.85 | 2.37 | 2.60 | 2.56 | 2.52 | 3.69 | 3.58 | 2.47 | 4.29 |
| U | 1.28 | 1.43 | 1.32 | 0.70 | 0.93 | 0.95 | 0.81 | 0.78 | 0.72 | 0.69 | 0.66 | 1.01 | 1.06 | 0.91 | 1.01 |

(*Continued*)

**Table 15.1.** *Major and trace element data for representative rocks from Aeolian volcanoes. Major element data for Vulcano and Panarea are from De Astis* et al. *(1997) and Calanchi* et al. *(2002) (Continued)*

| Sample | LIP 105 Lipari | LIP 113 Lipari | LIP 113B Lipari | LIP 114 Lipari | LIP 84 Lipari | LIP 182 Lipari | T17 Lipari | A3 LIP Lipari | LIP 180 Lipari | A16 LIP Lipari | MR6 Lipari | LIP 122 Lipari | LIP 143 Lipari | T9 Lipari | PN235 Panarea |
|---|---|---|---|---|---|---|---|---|---|---|---|---|---|---|---|
| $SiO_2$ | 52.31 | 52.64 | 52.64 | 53.38 | 53.53 | 53.54 | 53.59 | 53.76 | 53.82 | 54.08 | 54.94 | 55.19 | 57.05 | 59.27 | 47.83 |
| $TiO_2$ | 0.55 | 0.67 | 0.67 | 0.68 | 0.73 | 0.69 | 0.77 | 0.68 | 0.67 | 0.81 | 0.71 | 0.83 | 0.62 | 0.79 | 0.56 |
| $Al_2O_3$ | 14.90 | 14.95 | 14.95 | 14.97 | 16.56 | 17.19 | 17.00 | 16.72 | 17.80 | 17.25 | 17.81 | 16.28 | 17.41 | 16.18 | 17.50 |
| $Fe_2O_3$ | 8.62 | 9.16 | 9.16 | 9.13 | 9.17 | 8.99 | 9.60 | 9.35 | 8.59 | 8.67 | 9.01 | 9.35 | 8.33 | 8.14 | 8.94 |
| FeO | 0.00 | 0.00 | 0.00 | 0.00 | 0.00 | 0.00 | 0.00 | 0.00 | 0.00 | 0.00 | 0.00 | 0.00 | 0.00 | 0.00 | 0.00 |
| MnO | 0.14 | 0.19 | 0.19 | 0.32 | 0.14 | 0.17 | 0.16 | 0.16 | 0.15 | 0.14 | 0.16 | 0.15 | 0.17 | 0.15 | 0.14 |
| MgO | 7.69 | 6.48 | 6.48 | 5.80 | 4.60 | 4.58 | 4.74 | 5.24 | 4.50 | 4.42 | 4.03 | 4.17 | 3.79 | 3.42 | 5.64 |
| CaO | 10.83 | 10.38 | 10.38 | 10.04 | 9.67 | 8.87 | 9.42 | 8.88 | 8.12 | 8.89 | 8.48 | 8.84 | 7.62 | 6.47 | 9.32 |
| $Na_2O$ | 2.43 | 2.24 | 2.24 | 2.25 | 2.86 | 2.65 | 2.10 | 2.36 | 2.46 | 2.49 | 2.88 | 2.01 | 2.27 | 2.00 | 1.83 |
| $K_2O$ | 0.96 | 1.42 | 1.42 | 1.35 | 1.99 | 2.07 | 1.54 | 1.80 | 1.91 | 1.61 | 1.79 | 1.61 | 1.54 | 2.28 | 0.55 |
| $P_2O_5$ | 0.16 | 0.16 | 0.16 | 0.18 | 0.22 | 0.26 | 0.18 | 0.23 | 0.21 | 0.23 | 0.19 | 0.21 | 0.13 | 0.18 | 0.13 |
| LOI | 1.42 | 1.73 | 1.73 | 1.90 | 0.54 | 0.98 | 0.90 | 0.82 | 1.79 | 1.41 | 0.01 | 1.36 | 1.07 | 1.13 | 7.57 |
| V | 278 | 242 | 211 | 297 | 269 | 242 | 254 | 271 | 240 | 252 | 269 | 316 | 199 | 220 | 247 |
| Ga | 15 | 16 | 14 | 15 | 17 | 16 | 16 | 17 | 16 | 18 | 18 | 15 | 16 | 18 | 16 |
| Rb | 27 | 43 | 36 | 35 | 53 | 56 | 54 | 43 | 57 | 54 | 45 | 39 | 63 | 95 | 26 |
| Sr | 575 | 597 | 601 | 608 | 853 | 860 | 691 | 804 | 797 | 656 | 815 | 560 | 557 | 488 | 656 |
| Y | 15 | 20 | 19 | 18 | 19 | 18 | 19 | 17 | 19 | 21 | 17 | 19 | 25 | 23 | 19 |
| Zr | 45 | 64 | 67 | 62 | 86 | 81 | 90 | 71 | 78 | 91 | 77 | 67 | 75 | 120 | 58 |
| Nb | 2.3 | 4.4 | 3.9 | 4.0 | 7.1 | 6.6 | 6.1 | 5.2 | 6.6 | 6.2 | 5.1 | 4.3 | 5.8 | 8.8 | 4.1 |
| Cs | | | 1.02 | | 2.73 | 1.31 | 1.70 | 1.53 | 1.35 | 3.00 | | 2.51 | 2.09 | 3.62 | 0.76 |
| Ba | 316 | 329 | 344 | 356 | 526 | 481 | 392 | 464 | 444 | 555 | 478 | 366 | 373 | 620 | 281 |
| La | 13 | 17 | 18 | 18 | 24 | 24 | 22 | 22 | 23 | 23 | 20 | 18 | 25 | 27 | 17 |
| Ce | 25 | 35 | 36 | 37 | 49 | 48 | 46 | 43 | 45 | 48 | 41 | 37 | 48 | 56 | 33 |
| Pr | 2.8 | 3.7 | 3.8 | 4.3 | 5.3 | 5.2 | 5.2 | 5.0 | 5.2 | 5.4 | 4.7 | 4.1 | 5.3 | 5.9 | 4.0 |
| Nd | 13 | 17 | 18 | 19 | 23 | 23 | 23 | 21 | 23 | 23 | 21 | 19 | 22 | 26 | 19 |
| Sm | 3.11 | 3.75 | 4.14 | 3.43 | 5.75 | 5.14 | 4.60 | 3.34 | 4.85 | 5.07 | 3.94 | 4.83 | 5.55 | 4.97 | 4.20 |
| Eu | 0.80 | 1.16 | 0.98 | 0.96 | 1.14 | 1.47 | 1.13 | 1.03 | 1.31 | 1.43 | 1.23 | 1.35 | 1.32 | 1.17 | 1.08 |
| Gd | 4.01 | 4.25 | 3.47 | 3.83 | 4.00 | 4.36 | 4.67 | 4.19 | 4.00 | 4.60 | 4.11 | 3.44 | 4.35 | 4.23 | 3.89 |
| Tb | 0.48 | 0.58 | 0.61 | 0.55 | 0.58 | 0.58 | 0.67 | 0.63 | 0.59 | 0.61 | 0.51 | 0.43 | 0.62 | 0.60 | 0.51 |
| Dy | 2.61 | 3.50 | 3.59 | 3.58 | 3.81 | 3.56 | 4.21 | 3.63 | 3.38 | 3.96 | 3.26 | 3.57 | 4.25 | 4.15 | 3.33 |
| Ho | 0.55 | 0.66 | 0.67 | 0.61 | 0.62 | 0.65 | 0.89 | 0.55 | 0.65 | 0.83 | 0.67 | 0.64 | 0.74 | 0.80 | 0.68 |
| Er | 1.56 | 2.01 | 1.88 | 1.93 | 1.82 | 1.81 | 2.16 | 1.57 | 1.74 | 2.13 | 1.56 | 2.08 | 2.21 | 2.24 | 1.86 |
| Tm | | 0.25 | 0.29 | 0.34 | 0.34 | 0.24 | 0.32 | 0.33 | 0.28 | 0.40 | 0.29 | 0.29 | 0.42 | 0.35 | 0.26 |
| Yb | 1.81 | 1.91 | 1.85 | 1.98 | 1.96 | 1.67 | 1.99 | 1.65 | 1.67 | 2.35 | 1.53 | 1.97 | 2.35 | 2.11 | 1.61 |
| Lu | 0.45 | 0.29 | 0.27 | 0.51 | 0.29 | 0.26 | 0.31 | 0.35 | 0.27 | 0.39 | | 0.32 | 0.34 | 0.32 | 0.28 |
| Hf | 1.37 | 1.59 | 1.49 | 1.28 | 2.39 | 2.17 | 2.59 | 2.05 | 1.90 | 2.62 | 2.35 | 1.65 | 1.87 | 2.87 | 1.27 |
| Ta | 0.32 | 0.32 | 0.25 | 0.36 | 0.44 | 0.30 | 0.54 | 0.41 | 0.34 | 0.53 | 0.40 | 0.36 | 0.52 | 0.73 | 0.23 |
| Pb | 5.1 | 4.3 | 2.4 | 13.4 | 4.4 | 9.8 | 7.5 | 6.8 | 9.2 | 10.0 | 6.7 | 7.1 | 7.0 | 16.3 | 5.0 |
| Th | 2.80 | 3.89 | 3.85 | 4.02 | 5.44 | 5.70 | 5.79 | 6.03 | 5.45 | 5.95 | 5.05 | 4.28 | 4.94 | 8.70 | 3.90 |
| U | 0.86 | 1.16 | 0.99 | 1.25 | 1.80 | 1.47 | 1.61 | 1.66 | 1.63 | 1.54 | 1.53 | 1.66 | 1.41 | 2.27 | 0.56 |

| Sample | PF1 Panarea | PS 11A Panarea | VL168-10 Vulcano | VL250 Vulcano | VLPC1 Vulcano | VL229/1a + b Vulcano | VL143-1S Vulcano | VL145/2 Vulcano | VL272 Vulcano | VUL508 Vulcano | VL189/1 Vulcano | VL157/2 Vulcano | VL139-6 Vulcano | VL259/1 Vulcano | VL90/1 Vulcano |
|---|---|---|---|---|---|---|---|---|---|---|---|---|---|---|---|
| $SiO_2$ | 51.16 | 52.25 | 48.54 | 49.13 | 49.23 | 49.81 | 50.10 | 50.93 | 51.21 | 51.23 | 51.40 | 52.27 | 52.33 | 52.70 | 52.88 |
| $TiO_2$ | 0.62 | 0.92 | 0.77 | 0.66 | 0.68 | 0.68 | 0.76 | 0.76 | 0.67 | 0.81 | 0.69 | 0.70 | 0.80 | 0.71 | 0.71 |
| $Al_2O_3$ | 17.12 | 17.79 | 12.51 | 16.33 | 15.81 | 14.27 | 14.73 | 17.40 | 16.49 | 17.54 | 15.77 | 17.53 | 16.96 | 15.38 | 16.20 |
| $Fe_2O_3$ | 9.69 | 9.20 | 5.42 | 5.90 | 5.18 | 5.73 | 6.17 | 5.19 | 4.66 | 6.59 | 4.52 | 5.81 | 5.30 | 3.81 | 4.59 |
| FeO | 0.00 | 0.00 | 6.02 | 3.79 | 3.82 | 4.68 | 4.33 | 4.42 | 4.55 | 3.59 | 4.74 | 3.26 | 4.81 | 5.76 | 3.96 |
| MnO | 0.16 | 0.16 | 0.21 | 0.18 | 0.19 | 0.19 | 0.18 | 0.21 | 0.15 | 0.23 | 0.17 | 0.18 | 0.18 | 0.18 | 0.13 |
| MgO | 6.25 | 4.23 | 8.65 | 6.85 | 5.56 | 7.29 | 6.28 | 4.09 | 5.49 | 3.83 | 6.00 | 3.86 | 3.17 | 5.38 | 3.54 |
| CaO | 10.24 | 9.06 | 12.49 | 10.51 | 9.65 | 11.39 | 10.50 | 9.39 | 8.82 | 8.57 | 9.15 | 8.45 | 7.23 | 9.46 | 7.04 |
| $Na_2O$ | 2.54 | 2.50 | 2.20 | 2.31 | 3.10 | 2.40 | 1.77 | 2.44 | 2.83 | 3.33 | 2.69 | 3.13 | 3.32 | 2.71 | 4.35 |
| $K_2O$ | 0.90 | 2.45 | 2.08 | 1.75 | 3.78 | 2.04 | 2.23 | 2.52 | 2.47 | 2.72 | 2.56 | 2.63 | 3.67 | 2.46 | 3.36 |
| $P_2O_5$ | 0.08 | 0.58 | 0.21 | 0.25 | 0.48 | 0.22 | 0.22 | 0.28 | 0.27 | 0.28 | 0.26 | 0.29 | 0.40 | 0.21 | 0.39 |
| LOI | 1.24 | 0.85 | 0.90 | 2.33 | 2.53 | 1.30 | 2.72 | 2.37 | 2.39 | 1.29 | 2.06 | 1.89 | 1.82 | 1.23 | 2.83 |
| V | 251 | 341 | 264 | 260 | 228 | 237 | 245 | 208 | 253 | 326 | 245 | 213 | 251 | 211 | 195 |
| Ga | 16 | 20 | 15 | 15 | 18 | 19 | 12 | 16 | 20 | 16 | 17 | 18 | 17 | 16 | 16 |
| Rb | 21 | 82 | 46 | 17 | 115 | 47 | 58 | 58 | 35 | 51 | 57 | 50 | 113 | 60 | 125 |
| Sr | 593 | 893 | 1135 | 986 | 1619 | 1229 | 1077 | 1340 | 953 | 1293 | 1048 | 1249 | 1320 | 913 | 1303 |
| Y | 13 | 21 | 17 | 25 | 17 | 16 | 17 | 23 | 15 | 20 | 16 | 30 | 31 | 15 | 21 |
| Zr | 40 | 127 | 72 | 67 | 104 | 76 | 74 | 105 | 76 | 94 | 90 | 104 | 138 | 86 | 155 |
| Nb | 3.1 | 22.2 | 6.5 | 5.6 | 11.6 | 5.5 | 5.2 | 8.3 | 8.4 | 6.7 | 8.3 | 12.6 | 17.5 | 8.5 | 16.9 |
| Cs | 0.64 | 3.92 | 1.25 |  | 2.42 | 2.27 | 1.97 | 2.06 |  | 1.04 | 1.01 | 2.71 | 9.23 | 2.14 | 6.08 |
| Ba | 319 | 1199 | 578 | 567 | 1060 | 765 | 638 | 889 | 614 | 816 | 797 | 865 | 1150 | 630 | 1137 |
| La | 11 | 38 | 26 | 29 | 42 | 33 | 27 | 41 | 25 | 34 | 35 | 46 | 54 | 28 | 56 |
| Ce | 23 | 71 | 52 | 58 | 80 | 62 | 53 | 85 | 50 | 67 | 67 | 84 | 104 | 55 | 108 |
| Pr | 2.6 | 7.4 | 5.9 | 6.6 | 8.0 | 6.5 | 5.8 | 9.3 | 5.2 | 7.4 | 7.3 | 9.5 | 10.9 | 5.8 | 10.3 |
| Nd | 12 | 34 | 27 | 30 | 34 | 30 | 25 | 41 | 22 | 32 | 30 | 41 | 49 | 24 | 41 |
| Sm | 3.20 | 6.49 | 6.21 | 6.47 | 6.67 | 6.46 | 5.41 | 8.28 | 4.38 | 5.88 | 5.64 | 7.78 | 9.16 | 4.75 | 7.68 |
| Eu | 0.84 | 1.74 | 1.41 | 1.71 | 1.57 | 1.28 | 1.15 | 1.85 | 1.15 | 1.47 | 1.52 | 1.83 | 1.96 | 1.25 | 1.47 |
| Gd | 1.68 | 5.15 | 4.80 | 5.47 | 4.73 | 2.51 | 4.10 | 5.37 | 3.98 | 4.17 | 3.54 | 6.64 | 6.73 | 3.69 | 6.11 |
| Tb | 0.34 | 0.76 | 0.66 | 0.83 | 0.67 | 0.55 | 0.53 | 0.83 | 0.51 | 0.69 | 0.57 | 0.87 | 0.99 | 0.50 | 0.74 |
| Dy | 2.35 | 3.87 | 3.34 | 4.19 | 3.46 | 2.88 | 3.29 | 4.44 | 3.14 | 3.62 | 3.21 | 5.06 | 5.47 | 2.80 | 4.34 |
| Ho | 0.46 | 0.73 | 0.53 | 0.77 | 0.60 | 0.54 | 0.63 | 0.72 | 0.57 | 0.67 | 0.60 | 0.93 | 0.96 | 0.50 | 0.76 |
| Er | 1.41 | 2.03 | 1.61 | 2.08 | 1.48 | 1.66 | 1.62 | 2.00 | 1.57 | 1.96 | 1.65 | 2.73 | 2.66 | 1.30 | 1.88 |
| Tm | 0.22 | 0.27 | 0.23 | 0.31 | 0.27 | 0.38 | 0.25 | 0.25 |  | 0.27 | 0.20 | 0.45 | 0.33 | 0.23 | 0.36 |
| Yb | 1.26 | 1.64 | 1.19 | 1.80 | 1.66 | 1.16 | 1.29 | 1.69 | 0.97 | 1.55 | 1.34 | 2.17 | 2.01 | 1.27 | 1.87 |
| Lu | 0.25 | 0.26 |  | 0.29 | 0.18 | 0.23 | 0.21 | 0.29 | 0.30 | 0.30 | 0.22 | 0.40 | 0.37 | 0.22 | 0.30 |
| Hf | 1.02 | 3.16 | 1.81 | 1.46 | 2.01 | 1.95 | 2.06 | 2.25 | 1.94 | 2.41 | 2.37 | 2.60 | 3.01 | 1.99 | 3.49 |
| Ta | 0.16 | 0.91 | 0.32 | 0.27 | 0.51 | 0.29 | 0.23 | 0.48 | 0.42 | 0.47 | 0.39 | 0.63 | 1.14 | 0.48 | 1.23 |
| Pb | 5.2 | 13.9 | 8.3 | 7.1 | 13.2 | 9.3 | 7.7 | 13.4 | 9.5 | 9.1 | 11.6 | 13.7 | 18.0 | 11.5 | 17.9 |
| Th | 2.14 | 11.96 | 5.92 | 5.57 | 10.88 | 8.35 | 6.80 | 9.14 | 5.85 | 7.40 | 9.66 | 10.14 | 20.30 | 7.34 | 22.14 |
| U | 0.61 | 3.13 | 1.47 | 1.62 | 2.52 | 2.42 | 1.77 | 2.19 | 1.51 | 2.26 | 2.43 | 2.51 | 4.97 | 2.12 | 6.27 |

(*Continued*)

**Table 15.1.** *Major and trace element data for representative rocks from Aeolian volcanoes. Major element data for Vulcano and Panarea are from De Astis* et al. *(1997) and Calanchi* et al. *(2002) (Continued)*

| Sample | VL345/1 Vulcano | VL283/10 Vulcano | VL273/1 Vulcano | VL149/1 Vulcano | VL144/2 Vulcano | VL356/20 Vulcano | SC1 Stromboli | LS6 Stromboli | T2a Stromboli | At1 Stromboli | STR 13 Stromboli | LR 5 Stromboli | STR 11 Stromboli | STR 5 Stromboli | LS4 Stromboli |
|---|---|---|---|---|---|---|---|---|---|---|---|---|---|---|---|
| $SiO_2$ | 53.24 | 53.35 | 53.44 | 53.78 | 54.00 | 54.62 | 48.15 | 48.88 | 49.40 | 50.06 | 50.33 | 50.64 | 50.86 | 50.91 | 50.94 |
| $TiO_2$ | 0.86 | 0.67 | 0.63 | 0.69 | 0.75 | 0.66 | 0.93 | 0.84 | 0.99 | 0.95 | 0.81 | 1.00 | 0.91 | 0.90 | 0.97 |
| $Al_2O_3$ | 16.76 | 16.36 | 17.60 | 16.42 | 14.58 | 14.23 | 18.17 | 17.86 | 18.38 | 16.77 | 17.15 | 17.54 | 15.31 | 17.88 | 17.22 |
| $Fe_2O_3$ | 4.26 | 4.45 | 5.05 | 6.92 | 4.47 | 4.58 | 7.69 | 6.97 | 3.92 | 3.02 | 1.49 | 3.34 | 2.61 | 2.63 | 2.85 |
| FeO | 4.90 | 4.12 | 2.85 | 2.14 | 5.19 | 4.82 | 0.73 | 0.68 | 4.36 | 4.91 | 7.43 | 4.72 | 6.16 | 5.41 | 4.93 |
| MnO | 0.16 | 0.16 | 0.13 | 0.15 | 0.17 | 0.17 | 0.13 | 0.12 | 0.13 | 0.13 | 0.15 | 0.13 | 0.17 | 0.15 | 0.13 |
| MgO | 4.01 | 3.61 | 3.59 | 4.07 | 4.18 | 5.04 | 5.99 | 5.82 | 6.88 | 7.57 | 5.95 | 5.21 | 6.69 | 5.71 | 6.03 |
| CaO | 7.60 | 7.25 | 7.76 | 7.45 | 7.37 | 8.30 | 10.89 | 10.66 | 10.22 | 9.19 | 10.90 | 9.42 | 10.95 | 10.55 | 8.97 |
| $Na_2O$ | 2.63 | 4.17 | 4.38 | 3.35 | 2.98 | 2.84 | 2.31 | 2.38 | 2.77 | 2.19 | 2.55 | 2.59 | 2.23 | 2.45 | 2.49 |
| $K_2O$ | 2.83 | 4.36 | 2.53 | 3.59 | 4.57 | 3.39 | 1.82 | 1.72 | 1.81 | 3.63 | 2.33 | 3.53 | 3.23 | 2.33 | 3.77 |
| $P_2O_5$ | 0.27 | 0.36 | 0.34 | 0.30 | 0.36 | 0.25 | 0.48 | 0.44 | 0.40 | 0.63 | 0.60 | 0.61 | 0.65 | 0.53 | 0.67 |
| LOI | 2.49 | 1.14 | 1.70 | 1.14 | 1.38 | 1.11 | 2.71 | 3.65 | 0.74 | 0.95 | 0.31 | 1.26 | 0.23 | 0.55 | 1.05 |
| V | 220 | 199 | 194 | 238 | 231 | 199 | 220 | 220 | 258 | 220 | 262 | 247 | 257 | 247 | 221 |
| Ga | 18 | 16 | 15 | 15 | 15 |  | 15 | 14 | 14 | 13 | 15 | 15 | 15 | 17 | 15 |
| Rb | 68 | 144 | 79 | 102 | 136 | 136 | 62 | 60 | 50 | 117 | 70 | 124 | 108 | 64 | 101 |
| Sr | 1115 | 1162 | 1275 | 1041 | 1345 | 980 | 783 | 707 | 643 | 792 | 674 | 894 | 745 | 662 | 749 |
| Y | 20 | 21 | 16 | 23 | 24 | 25 | 24 | 23 | 22 | 24 | 22 | 27 | 26 | 21 | 24 |
| Zr | 109 | 139 | 100 | 104 | 143 | 145 | 151 | 145 | 106 | 165 | 140 | 168 | 145 | 136 | 165 |
| Nb | 11.7 | 17.4 | 9.9 | 12.3 | 14.2 | 10.0 | 17.5 | 16.2 | 13.0 | 19.3 | 21.5 | 23.8 | 27.1 | 24.3 | 20.5 |
| Cs | 2.57 | 5.60 | 1.97 | 2.04 | 5.07 | 5.58 | 4.91 | 5.65 | 2.09 | 5.44 | 3.18 | 4.39 | 7.30 | 4.36 | 7.13 |
| Ba | 701 | 993 | 862 | 746 | 980 | 600 | 1030 | 953 | 815 | 1660 | 995 | 1851 | 1553 | 891 | 1707 |
| La | 32 | 51 | 34 | 41 | 51 | 53 | 43 | 42 | 36 | 47 | 42 | 54 | 53 | 45 | 45 |
| Ce | 63 | 95 | 62 | 82 | 99 | 98 | 92 | 86 | 75 | 101 | 91 | 110 | 111 | 88 | 95 |
| Pr | 6.6 | 9.6 | 6.2 | 8.5 | 10.2 | 10.0 | 9.9 | 9.2 | 7.5 | 11.2 | 9.9 | 11.5 | 12.5 | 9.4 | 10.5 |
| Nd | 29 | 38 | 29 | 37 | 42 | 33 | 40 | 41 | 32 | 47 | 41 | 51 | 49 | 39 | 47 |
| Sm | 5.70 | 7.73 | 5.29 | 7.22 | 8.27 | 7.50 | 6.90 | 8.22 | 6.36 | 9.95 | 8.79 | 10.14 | 11.36 | 7.41 | 9.10 |
| Eu | 1.45 | 1.63 | 1.44 | 1.51 | 1.60 | 1.39 | 1.88 | 1.59 | 1.50 | 1.79 | 2.22 | 1.87 | 2.77 | 2.12 | 2.04 |
| Gd | 4.18 | 5.41 | 3.32 | 4.98 | 5.68 | 4.00 | 5.43 | 5.90 | 4.98 | 7.08 | 4.78 | 8.10 | 8.61 | 5.71 | 7.36 |
| Tb | 0.65 | 0.67 | 0.55 | 0.76 | 0.90 | 0.78 | 0.89 | 0.78 | 0.81 | 0.99 | 0.79 | 1.05 | 1.15 | 0.78 | 0.88 |
| Dy | 3.61 | 3.83 | 2.90 | 4.16 | 4.67 | 3.95 | 4.55 | 4.69 | 4.34 | 5.33 | 4.24 | 5.47 | 5.50 | 4.39 | 4.91 |
| Ho | 0.66 | 0.64 | 0.49 | 0.75 | 0.77 | 0.69 | 0.83 | 0.80 | 0.78 | 0.87 | 0.94 | 1.04 | 1.02 | 0.86 | 0.81 |
| Er | 1.83 | 1.81 | 1.30 | 1.91 | 2.20 | 1.83 | 2.17 | 2.16 | 1.88 | 2.28 | 2.35 | 2.47 | 2.61 | 2.05 | 2.18 |
| Tm | 0.28 | 0.26 | 0.22 | 0.25 | 0.31 | 0.29 | 0.27 | 0.37 | 0.40 | 0.32 | 0.32 | 0.39 | 0.36 | 0.31 | 0.33 |
| Yb | 1.91 | 1.97 | 1.18 | 1.50 | 1.98 | 2.20 | 2.52 | 2.06 | 2.08 | 1.95 | 2.02 | 2.12 | 2.56 | 2.28 | 1.48 |
| Lu | 0.25 | 0.25 | 0.23 | 0.29 | 0.29 | 0.33 | 0.32 | 0.26 | 0.26 | 0.31 | 0.34 | 0.35 | 0.40 | 0.30 | 0.30 |
| Hf | 2.91 | 3.26 | 2.01 | 2.51 | 3.83 | 3.60 | 3.40 | 3.41 | 2.43 | 4.11 | 2.57 | 3.49 | 3.87 | 3.29 | 3.54 |
| Ta | 0.66 | 0.97 | 0.42 | 0.81 | 0.95 | 0.90 | 1.11 | 1.11 | 0.52 | 1.15 | 0.66 | 1.52 | 0.98 | 0.86 | 1.32 |
| Pb | 12.6 | 17.4 | 11.3 | 16.8 | 18.7 | 16.0 | 26.0 | 39.5 | 20.5 | 23.3 | 18.3 | 25.2 | 25.7 | 15.8 | 23.5 |
| Th | 8.27 | 21.06 | 8.30 | 14.03 | 19.73 | 18.00 | 15.16 | 14.69 | 11.03 | 19.20 | 14.48 | 18.29 | 15.43 | 13.58 | 18.49 |
| U | 2.40 | 6.20 | 2.26 | 4.20 | 5.55 | 5.30 | 3.52 | 3.14 | 3.08 | 5.23 | 3.90 | 4.96 | 3.52 | 3.72 | 5.14 |

| Sample | STR 9 Stromboli | LS3 Stromboli | STR 12 Stromboli | STR 16 Stromboli | L2e Stromboli | STR 7 Stromboli | STR 6 Stromboli | STR 1 Stromboli | STR 2 Stromboli | STR 4 Stromboli | STR 3 Stromboli | STR 15 Stromboli | T3b1 Stromboli | STR 77 Stromboli | STR 17 Stromboli | STR 10 Stromboli | STR 8 Stromboli |
|---|---|---|---|---|---|---|---|---|---|---|---|---|---|---|---|---|---|
| $SiO_2$ | 50.99 | 51.10 | 51.12 | 51.20 | 51.31 | 51.31 | 51.33 | 51.70 | 51.81 | 52.05 | 52.32 | 52.43 | 52.57 | 52.63 | 52.63 | 53.66 | 55.36 |
| $TiO_2$ | 0.96 | 0.93 | 0.89 | 0.88 | 0.78 | 0.95 | 0.95 | 0.95 | 0.83 | 0.91 | 0.72 | 0.90 | 0.88 | 0.93 | 0.95 | 0.7 | 0.63 |
| $Al_2O_3$ | 17.92 | 17.63 | 16.93 | 16.70 | 18.57 | 18.39 | 17.33 | 17.78 | 17.66 | 17.88 | 18.00 | 16.56 | 17.43 | 16.58 | 16.59 | 15.45 | 15.33 |
| $Fe_2O_3$ | 2.55 | 2.56 | 2.00 | 8.99 | 2.04 | 2.17 | 2.55 | 3.03 | 1.18 | 1.90 | 1.33 | 8.24 | 4.35 | 2.70 | 2.57 | 3.01 | 2.23 |
| FeO | 7.11 | 4.76 | 6.33 | 0.00 | 4.99 | 7.37 | 5.91 | 5.07 | 6.07 | 5.53 | 5.91 | 0.00 | 2.93 | 5.09 | 6.02 | 6.11 | 5.63 |
| MnO | 0.18 | 0.13 | 0.13 | 0.16 | 0.12 | 0.17 | 0.16 | 0.16 | 0.15 | 0.16 | 0.15 | 0.15 | 0.13 | 0.15 | 0.15 | 0.19 | 0.17 |
| MgO | 4.10 | 6.09 | 5.43 | 6.30 | 7.12 | 3.75 | 4.28 | 4.77 | 5.82 | 5.10 | 6.69 | 4.92 | 6.18 | 5.71 | 4.89 | 5.88 | 6.23 |
| CaO | 10.21 | 8.66 | 9.59 | 11.24 | 9.62 | 8.99 | 9.32 | 8.80 | 8.88 | 9.00 | 10.09 | 9.08 | 9.17 | 9.11 | 9.16 | 10.2 | 9.86 |
| $Na_2O$ | 2.43 | 3.02 | 2.33 | 2.47 | 2.61 | 3.15 | 2.55 | 2.51 | 2.23 | 2.43 | 2.11 | 2.59 | 2.89 | 2.39 | 2.55 | 2.31 | 2.3 |
| $K_2O$ | 2.00 | 3.43 | 3.91 | 2.30 | 1.69 | 2.83 | 4.09 | 3.49 | 4.57 | 3.72 | 1.77 | 3.75 | 2.00 | 3.63 | 3.79 | 1.5 | 1.55 |
| $P_2O_5$ | 0.32 | 0.61 | 0.63 | 0.52 | 0.29 | 0.50 | 0.71 | 0.71 | 0.53 | 0.62 | 0.25 | 0.59 | 0.36 | 0.59 | 0.55 | 0.15 | 0.16 |
| LOI | 1.23 | 1.08 | 0.70 | 0.23 | 0.87 | 0.43 | 0.83 | 1.03 | 0.27 | 0.71 | 0.66 | 0.22 | 1.11 | 0.48 | 0.16 | 0.83 | 0.55 |
| V | 219 | 242 | 242 | 250 | 227 | 227 | 219 | 226 | 225 | 233 | 217 | 243 | 212 | 242 | 246 | 218 | 238 |
| Ga | 17 | 14 | 15 | 18 | 13 | 16 | 17 | 16 | 14 | 16 | 13 | 19 | 15 | 16 | 21 | 13 | 16 |
| Rb | 59 | 108 | 112 | 68 | 55 | 88 | 113 | 104 | 126 | 113 | 50 | 128 | 56 | 110 | 126 | 44 | 58 |
| Sr | 663 | 805 | 848 | 812 | 482 | 709 | 729 | 806 | 627 | 755 | 429 | 741 | 636 | 692 | 764 | 516 | 553 |
| Y | 21 | 25 | 24 | 26 | 19 | 24 | 21 | 23 | 18 | 22 | 16 | 33 | 24 | 25 | 28 | 16 | 18 |
| Zr | 138 | 159 | 163 | 164 | 95 | 164 | 163 | 173 | 142 | 152 | 85 | 204 | 139 | 161 | 197 | 91 | 106 |
| Nb | 19.6 | 23.2 | 33.2 | 22.5 | 10.8 | 27.4 | 28.2 | 36.8 | 27.1 | 30.3 | 12.3 | 28.0 | 13.9 | 20.1 | 27.4 | 10.1 | 17.7 |
| Cs | 3.48 | 6.73 | 5.47 | 3.13 | 3.65 | 3.48 | 7.68 | 7.72 | 6.16 | 7.60 | 3.48 | 3.89 | 1.67 | 2.07 | 6.23 | 2.15 | 3.28 |
| Ba | 757 | 1722 | 1815 | 1226 | 725 | 1206 | 1570 | 1825 | 1360 | 1611 | 656 | 1682 | 812 | 1450 | 1683 | 465 | 648 |
| La | 45 | 50 | 57 | 48 | 25 | 50 | 49 | 58 | 43 | 57 | 25 | 54 | 42 | 44 | 54 | 27 | 33 |
| Ce | 90 | 102 | 122 | 99 | 52 | 96 | 101 | 116 | 89 | 120 | 49 | 119 | 82 | 89 | 112 | 52 | 62 |
| Pr | 9.4 | 10.8 | 13.3 | 10.5 | 5.2 | 10.5 | 11.2 | 12.5 | 9.4 | 13.3 | 5.5 | 12.5 | 8.2 | 9.7 | 11.9 | 5.6 | 6.9 |
| Nd | 38 | 49 | 52 | 47 | 23 | 40 | 47 | 52 | 42 | 53 | 22 | 55 | 35 | 44 | 49 | 22 | 27 |
| Sm | 6.85 | 9.13 | 10.08 | 8.33 | 4.40 | 7.95 | 10.05 | 9.86 | 8.02 | 10.44 | 4.64 | 9.95 | 6.65 | 8.60 | 10.12 | 3.72 | 5.16 |
| Eu | 1.71 | 2.16 | 2.48 | 1.96 | 1.21 | 2.10 | 2.35 | 2.60 | 2.39 | 2.56 | 1.36 | 2.40 | 1.36 | 1.98 | 2.39 | 1.11 | 1.59 |
| Gd | 5.50 | 7.19 | 7.25 | 6.72 | 4.39 | 6.75 | 7.63 | 7.21 | 6.71 | 7.51 | 4.04 | 7.54 | 4.83 | 5.30 | 6.54 | 3.71 | 4.23 |
| Tb | 0.72 | 1.00 | 0.97 | 1.04 | 0.62 | 0.81 | 0.91 | 0.97 | 0.83 | 1.00 | 0.59 | 1.20 | 0.71 | 0.87 | 1.11 | 0.5 | 0.63 |
| Dy | 4.40 | 5.28 | 4.89 | 4.98 | 3.69 | 4.52 | 4.48 | 5.22 | 4.14 | 4.83 | 3.14 | 6.82 | 4.79 | 5.14 | 5.09 | 2.84 | 3.35 |
| Ho | 0.83 | 0.99 | 0.98 | 0.93 | 0.71 | 0.87 | 0.85 | 0.95 | 0.69 | 0.88 | 0.65 | 1.15 | 0.85 | 0.89 | 0.94 | 0.56 | 0.66 |
| Er | 2.30 | 2.31 | 2.17 | 2.28 | 1.69 | 2.31 | 2.11 | 2.29 | 1.86 | 2.27 | 1.66 | 3.19 | 2.15 | 2.47 | 2.80 | 1.6 | 1.72 |
| Tm | 0.35 | 0.29 | 0.32 | 0.51 | 0.28 | 0.30 | 0.28 | 0.28 | 0.26 | 0.31 | 0.23 | 0.69 | 0.38 | 0.32 | 0.44 | 0.25 | 0.3 |
| Yb | 2.32 | 1.86 | 2.07 | 2.04 | 1.92 | 2.39 | 2.05 | 2.15 | 1.83 | 1.80 | 1.53 | 2.49 | 1.99 | 1.99 | 2.44 | 1.68 | 1.84 |
| Lu | 0.33 | 0.28 | 0.26 | 0.38 | 0.22 | 0.32 | 0.25 | 0.30 | 0.24 | 0.32 | 0.28 | 0.56 | 0.39 | 0.40 | 0.48 | 0.26 | 0.28 |
| Hf | 3.19 | 3.85 | 4.08 | 3.30 | 2.04 | 3.68 | 4.09 | 3.84 | 3.27 | 3.51 | 2.10 | 5.19 | 2.77 | 3.77 | 4.43 | 2.51 | 2.51 |
| Ta | 0.72 | 1.30 | 1.33 | 0.79 | 0.56 | 0.84 | 0.91 | 1.23 | 0.83 | 1.06 | 0.46 | 1.10 | 0.89 | 1.16 | 1.19 | 0.34 | 0.47 |
| Pb | 13.3 | 23.4 | 29.5 | 22.0 | 12.8 | 19.1 | 27.5 | 29.8 | 19.1 | 26.1 | 12.8 | 21.3 | 11.2 | 16.5 | 25.4 | 9.9 | 15.2 |
| Th | 12.65 | 16.17 | 16.94 | 17.64 | 10.34 | 17.58 | 18.96 | 17.85 | 16.02 | 15.70 | 9.19 | 20.42 | 14.10 | 17.43 | 20.69 | 7.02 | 9.51 |
| U | 3.06 | 4.39 | 5.24 | 3.96 | 2.96 | 4.31 | 5.63 | 4.93 | 5.29 | 3.86 | 2.37 | 5.96 | 2.98 | 4.49 | 5.58 | 2.04 | 2.71 |

Analyses have been carried out by LA-ICPMS at the Department of Earth Sciences, University of Perugia, using a New Wave UP213 LA system coupled with a Thermo Electron X7 (Thermo Electron Corporation, Waltham, USA) ICP-MS. A 60 micrometres laser beam has been used. Details on analytical methods are reported by Petrelli *et al*. (2007, 2008). Precision expressed as standard relative deviation is better that 5% for almost all elements, except Cr and Ho (>7%).

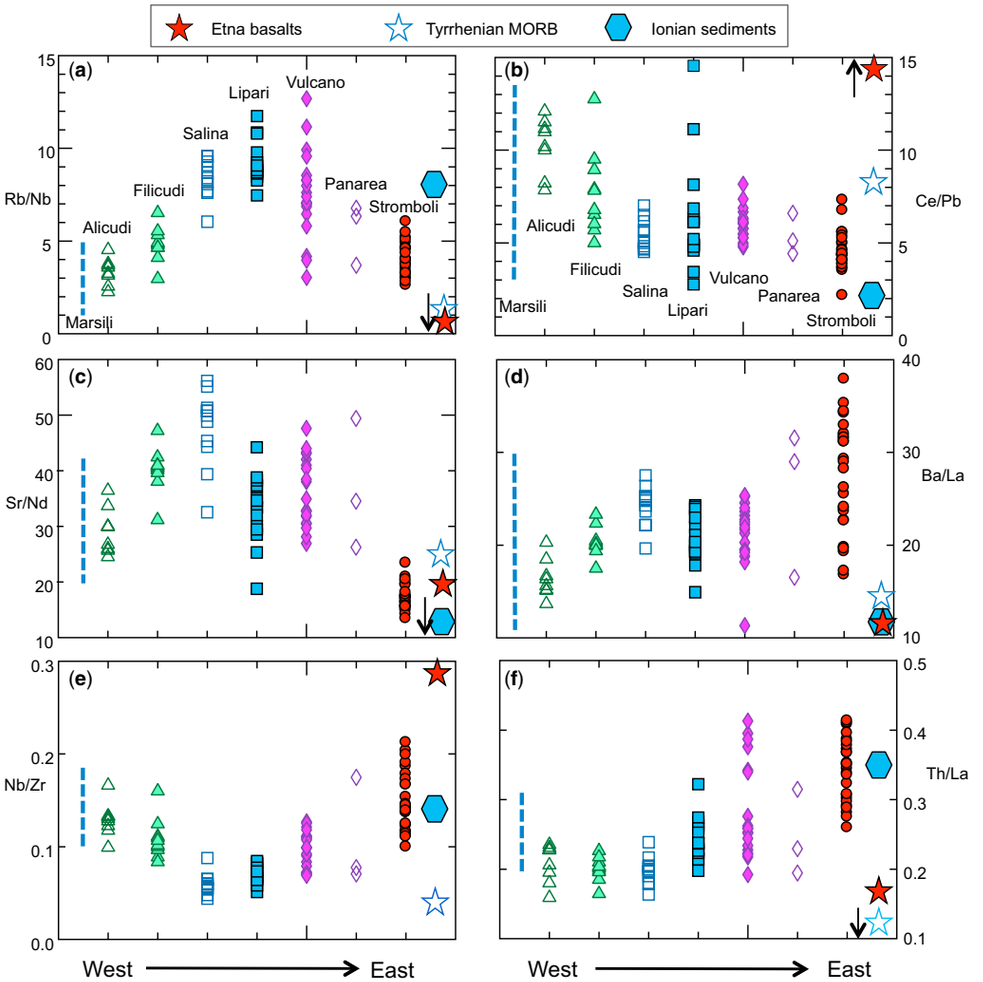


**Fig. 15.9.** Regional variation of trace element ratios for the newly analysed Aeolian samples (Table 15.1). Average compositions of Tyrrhenian MORB (Dietrich *et al.* 1977), Etna (Viccaro & Cristofolini 2008) and Ionian sediments (De Astis, unpublished data) are also reported.

along-arc variation of some ITE ratios is reported in Figure 15.9. The predominant features observed on diagrams are as follows.

(1) There is an evident increase of Rb/Nb and several other LILE/HFSE ratios (e.g. La/Nb, Ba/Nb, U/Nb and, to a lesser extent, Rb/Ta) from the marginal islands of Alicudi and Stromboli to the central islands, where a large scattering is observed for Vulcano.
(2) LILE/LILE ratios also show considerable variation along the arc. For instance, Ce/Pb decreases eastwards and exhibits a large scattering at Lipari. Sr/Nd and Sr/Th (not shown) ratios are lower at the arc margins, especially at Stromboli, than in the central islands (Fig. 15.9c). Ba/La increases from Alicudi to Filicudi and other central islands, reaching a maximum at Stromboli which also shows a large range of values (Fig. 15.9d).
(3) HFSE/HFSE ratios Nb/Zr (Fig. 15.9e), Zr/Ti and, to a lesser extent, Nb/Ta (not shown) decrease from marginal to central islands. Nb and Zr abundances, but also LREE abundances and La/Yb ratios, show the same type of distribution (not shown).
(4) Th/LREE ratios (Fig. 15.9f) remain fairly constant in the CA rocks of the western-central arc and increase in the Vulcano shoshonitic rocks and at Stromboli.
(5) The Marsili volcano, sited in a back-arc position NW of the Aeolian archipelago, shows a wide range of compositions but is close to the western island of Alicudi for many ITE ratios.

Most trace element ratios of Figure 15.9 are not affected by fractional crystallization since they are equally incompatible in the main igneous rock minerals. Also, they do not show significant correlation with Sr isotopes in the contaminated Alicudi and Primordial Vulcano mafic suites. It is therefore reasonable to conclude that the observed along-arc variations reflect a compositional zoning of the mantle source. Understanding the processes that generated these variations is crucial for clarifying key aspects of the Aeolian subduction factory.

### *Mantle metasomatism*

At least three different end-members are considered to have contributed to the source composition of the Aeolian magmas. These include the pre-metasomatic mantle, the Ionian subducted crust and the Ionian Sea sediments. The composition of each end-member is internally variable and poorly known. The upper mantle beneath the southern Tyrrhenian Sea has a mid-ocean-ridge basalt (MORB-) to OIB-type composition, based on geochemistry of magmas erupted in and around the Tyrrhenian Sea basin (Trua *et al.* 2004, 2011). Subducted Ionian crust has been hypothesized to have an oceanic to thinned continental character, and a lateral variation in composition has been suggested (Doglioni *et al.* 2001). Sediments are abundant on the Ionian seafloor, but inadequately characterized compositionally. For this reason, a geochemical study of Ionian sediments has been undertaken and preliminary data are reported as a spider-diagram in Figure 15.5d.

The concomitant increase of Sr- and decrease of Nd-isotope ratios from the western to eastern Aeolian arc have been interpreted as evidence for eastwards increasing contamination of the mantle source by subducted upper crustal material, likely

sediments (e.g. Ellam *et al.* 1988, 1989; Francalanci *et al.* 1993, 2004, 2007; De Astis *et al.* 2000; Peccerillo 2005). The new analyses of Ionian sediments show Sr concentrations of *c.* 200 ppm and $^{87}Sr/^{86}Sr$ of *c.* 0.711. Assuming a bulk mixing between a primordial-type mantle and such sediments, an addition of less than 2% contaminant is sufficient to explain the entire range of isotopic variation along the western-central Aeolian arc (Fig. 15.7). Much higher amounts of *c.* 4–10% are necessary to explain the composition of the Stromboli mantle sources. These are maximum values because shallow-level magma contamination likely contributed to increase Sr isotope ratios of Aeolian magmas, including the mafic magmas. Moreover, bulk mixing is not a viable mechanism of mantle contamination, and hydrous fluid or melts from sediments have been suggested as the likely carriers of incompatible elements into the mantle wedge (Hermann & Rubatto 2009). These are much richer in Sr than the source rocks because of low solid/fluid partition coefficients for Sr at high pressures (Hermann & Rubatto 2009). This considerably decreases the amount of contaminant that would be necessary to explain the Sr-isotope ratios observed along the arc. For instance, if a melt formed by 30–50% sediment melting is assumed as metasomatic agent, Sr concentration in the melt would be 2–3 times higher than the source rock. This reduces the amount of mantle contaminant by a factor of 2–3, and less than 1% melted sediment is sufficient to explain Sr-isotope ratios of the western-central arc and only 2–5% would be needed at Stromboli.

In conclusion, two types of metasomatic agents, likely fluids, are suggested by Sr-isotope modelling in the Aeolian arc. One type of fluid, operating in the western-central arc, had low Sr isotope ratios and was likely released from an oceanic slab with little or no sediment involvement. Another fluid was enriched in radiogenic Sr and requires an important contribution from sediments in the eastern sector of the arc. Following Hermann & Rubatto (2009), the term 'fluid' is used here in its broadest sense, that is, to indicate aqueous fluids (water-rich fluid containing low amount of solute), $H_2O$-rich silicate melts and supercritical $H_2O$-silicic fluids (intermediate between the two).

The hypothesis of two compositionally distinct metasomatic fluids is supported by incompatible trace element ratios such as Ba/La, Th/Sr, Th/Pb, Th/U, Ba/La, Ti/Zr and Sr/Nd, which all show diverging trends for Stromboli and for the central-western islands (e.g. De Astis *et al.* 2000). Variations for some of these ratios are reported in Figure 15.10

The nature of metasomatic fluids and the efficiency of element transfer from slab to the mantle wedge is controversial. This is true not only for the Aeolian arc, but for subduction magmatism at a global scale (Brenan *et al.* 1995; Elliot *et al.* 1997; Becker *et al.* 2000; Kessel *et al.* 2005; Hermann & Rubatto 2009).

Investigation of MORB-type rocks (Kessel *et al.* 2005) demonstrated that the capacity of elemental transport increases with increasing temperature and pressure from aqueous fluids to supercritical fluids and melts. LILE/LILE ratios such as Rb/Sr, Ba/La and Ba/Rb are more easily fractionated by aqueous fluids than by high-temperature supercritical fluids and melts. However, hydrous melts and supercritical fluids more efficiently fractionate other element ratios such as Sr/REE and La/Yb. LILE/HFSE are fractionated by all types of fluids, but low-temperature aqueous fluids are less able to transfer large amounts of trace elements than high-temperature supercritical fluids and melts. High LILE/HFSE ratios coupled with low ITE abundances (e.g. Th) have therefore been suggested as useful criteria to recognize aqueous fluid metasomatic modifications (Kessel *et al.* 2005).

Hermann & Rubatto (2009) suggested that subducted sediments are the most important sources of incompatible elements for metasomatic fluids in subduction zones. The involvement of sediments in the subduction processes considerably complicates the process of slab to mantle element transfer however, due to the possible occurrence of a large variety of major and accessory residual phases such as phengite, rutile, allanite/monazite and zircon. Their stability or breakdown at various pressure/temperature (P/T) conditions influences the composition of fluids emitted from the slab and hence the flux of incompatible trace elements into the overlying mantle wedge. For instance, two- to five-fold Ba/La variations can be generated in melted sediments and transferred to the mantle wedge from these, depending on the occurrence or absence of phengite and monazite in the residue. Note that high Ba/La is traditionally considered a typical signature of low-temperature metasomatic aqueous fluids (Brenan *et al.* 1995; Elliott *et al.* 1997).

The intrinsic complexities of element transfer from slab to mantle wedge, along with the poorly known compositions of end-members involved in the Aeolian subduction processes, make it difficult to understand mechanisms of element mobilization and the contribution of various components to mantle wedge composition. This has fed much speculation and debate; for example, Tonarini *et al.* (2004) suggested an increase of both aqueous fluid flow and sediment input from west to the east, on the basis of an eastwards increase of B/Nb and $\delta^{11}B$ of lavas. This is supported by an eastwards decrease of Ce/Pb, typical of aqueous fluids, and an increase in Th/La, which is high in the sediments (Fig. 15.9f). However, LILE/HFSE show a decrease from central arc to Stromboli, that is, the opposite to that expected for aqueous fluid metasomatism.

Francalanci *et al.* (1993, 2007) argued that an increase of LILE/HFSE from external to central islands was related to a stronger role of metasomatism by aqueous fluids in the central arc. However, this idea only holds if a homogeneous composition of pre-metasomatic mantle wedge is assumed for LILE/HFSE. Moreover, high mobile/immobile element ratios (e.g. Rb/Th) should be coupled with low immobile element (e.g. Th) enrichments (Kessel *et al.* 2005). This is not observed in the central Aeolian arc, except perhaps at Salina. Finally, variations of HFSE/HFSE

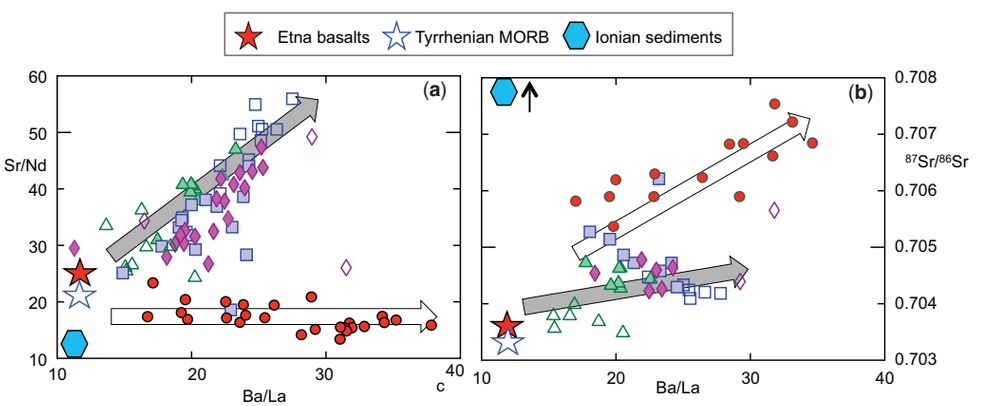


**Fig. 15.10.** Ba/La, Sr/Nd and $^{87}Sr/^{86}Sr$ variation diagrams for the newly analysed rocks. Sr isotope data are from the literature (source of data as in Fig. 15.2) and have been determined either on the same rocks analysed in this study or on different rock samples from the same outcrops. Composition of the Tyrrhenian MORB, Etna and Ionian sediments are also reported. Arrows indicate effects of metasomatic fluids derived from oceanic crust (grey arrow) and from sediments (white arrow). Symbols as in Figure 15.4.

ratios (Fig. 15.9e) are also difficult to explain, in that this group of elements is immobile during aqueous fluid transfer. Therefore, aqueous fluid transfer may have been present in the central Aeolian arc, but it cannot be the only process responsible for the observed trace element variations.

Many of the issues mentioned above are overcome if a heterogeneous OIB- to MORB-type starting mantle composition is assumed for the Aeolian arc (Ellam *et al.* 1988). An OIB-type component under the external islands could explain enrichment in Nb and LREE, as well as the relatively high Nb/Zr and low Rb/Nb and Sr/Nd ratios. By contrast, a MORB-type composition for the central arc better explains the low Nb/Zr and Zr/Ti.

However, several issues still remain unresolved. For instance, variations of Ba/La (Fig. 15.10) cannot result from any shallow-level magmatic evolution process. By contrast, Sr/Nd ratios can change during crystal fractionation if plagioclase is involved; however, the positive correlation with Ba/La in the western-central islands excludes this possibility (Fig. 15.10a). The covariation of Ba/La and Sr/Nd in the central-western arc is therefore a reproduction of source heterogeneity, and can be attributed to metasomatic fluids from an oceanic slab (grey arrows in Fig. 15.10). The slight positive trend between Sr/Nd and $^{87}Sr/^{86}Sr$ could indicate modest sediment involvement, but might also reflect a variably altered oceanic crust as source of fluids. Positive correlation between Ba/La and $^{87}Sr/^{86}Sr$ at Stromboli fits well with the hypothesis of metasomatism by low-temperature (about 700–800 °C) hydrous melts from sediments (white arrows in Fig. 15.10), which have high Ba/La because of residual LREE-rich accessory phases (Hermann & Rubatto 2009). However, experimental data clearly show that these melts also have high Sr/Nd, and a positive correlation between the two ratios should be observed. Instead, the almost flat trend for Stromboli rocks (Fig. 15.10a) requires a selective Ba enrichment that increases Ba/La but not Sr/Nd and other ITE ratios. Tommasini *et al.* (2007) suggested a two-stage enrichment process for the Stromboli mantle an hypothesis supported by Schiavi *et al*. (2012) on the basis of trace element and Pb-B-Li isotope data on melt inclusions. Early high-P/T supercritical fluids from basalts and sediments produced a general enrichment in all lithophile elements, with little element fractionation. An aqueous fluid at lower P/T selectively enriched the mantle wedge in Ba (see Francalanci *et al.* 2013). However, other element ratios that are strongly affected by fluid transport (e.g. U/Nb, Rb/Th, U/Ta, U/Th, etc.) should be correlated with Ba/La, a feature that is not observed in the Stromboli rocks.

### *Conditions of mantle melting and the origin of calc-alkaline and shoshonitic magmas*

The distribution of calc-alkaline and shoshonitic magmas in space and time has received considerably less attention in the literature than trace elements and isotope geochemistry. Calc-alkaline rocks have comparable composition as shoshonites for several major and trace elements (Fig. 15.3), but shoshonites have higher concentrations of K, P and all incompatible trace elements. Some shoshonites are undersaturated in silica, with up to 10% of normative nepheline, whereas calc-alkaline rocks are saturated to oversaturated in silica. These differences can depend either on a heterogeneous source and/or on variable degrees and physico-chemical conditions of partial melting.

REE geochemistry can help to clarify this issue. Light REE fractionation (i.e. La/Sm) of primary magmas depends on the degree of melting and/or on the La enrichment of the source. Heavy REE (HREE) fractionation (i.e. Tb/Yb) depends essentially on the presence or absence of residual garnet during mantle melting. Garnet is a high-pressure mantle mineral that retains HREE with respect to the light and mid REE. Its occurrence as residual phase during partial melting therefore results in high Tb/Yb (and La/Yb) in the magmas. La/Sm increases slightly with magma evolution; only mafic rocks should therefore be considered for constraining source processes.

The La/Sm v. $K_2O$ diagram for the most mafic among the analysed rocks (MgO >4 wt%) shows that Filicudi, Salina and Lipari have similar La/Sm ratios, but higher values are observed at Alicudi and in some CA samples from Stromboli (Fig. 15.11a). Since all these rocks have the same petrological characteristics, it is reasonable to assume an origin by comparable degrees of mantle melting. Higher La/Sm ratios in the CA rocks of the two external islands therefore point to a stronger enrichment of LREE in their mantle sources. At Vulcano, there is an increase of La/Sm from CA to SHO rocks at fairly constant Sr-isotope ratio (De Astis *et al.* 1997). By contrast, La/Sm ratios do not change significantly from CA to SHO rocks at Stromboli, whereas $^{87}Sr/^{86}Sr$ ratios increase strongly (Francalanci *et al.* 1988). These data suggest that HKCA and SHO magmas at Vulcano could be related to variable degrees of partial melting of a homogeneous source, whereas CA and SHO magmas at Stromboli are generated by similar degrees of partial melting of a isotopically heterogeneous source that was variably contaminated by subducted sediments. The obvious conclusion is that SHO magmas are generated by different processes in the Aeolian arc as already suggested by Ellam *et al.* (1988) and De Astis *et al.* (2000). Finally, Tb/Yb ratios are generally high in all shoshonites. This points to the occurrence of residual garnet in the source during melting and, hence, to a deeper origin for SHO than the associated CA magmas.

The physical conditions that generated variable degrees of melting for CA and SHO magmas in the central Aeolian arc are of interest for petrology and geodynamics. It is well known that water is crucial to promote partial melting in the subduction environments (e.g. Ulmer 2001; Grove *et al*. 2012). Variable degrees of melting in the Aeolian arc could therefore be related to different fluxes of water from the slab. These were higher

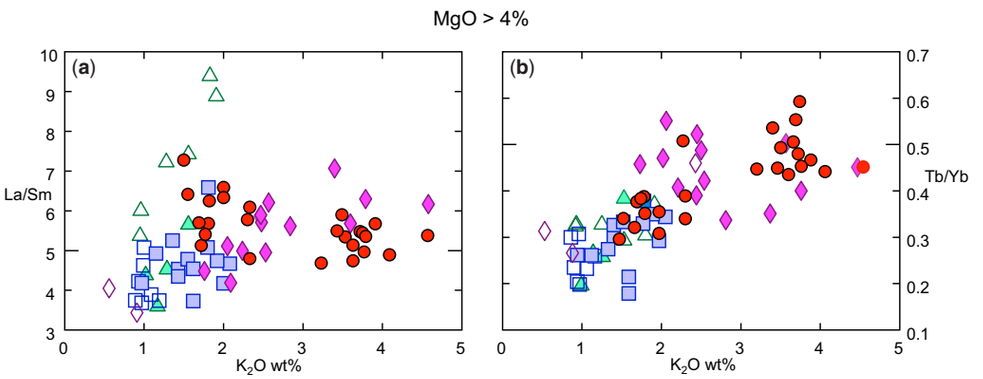


**Fig. 15.11.** La/Sm and Tb/Yb v. $K_2O$ diagrams for the most mafic among the analysed samples (MgO > 4 wt%). Plots are restricted to mafic compositions to minimize effects of La/Sm variation related to fractional crystallization. For further explanation see text. Symbols as in Figure 15.4.

during calc-alkaline magma activity, and were less abundant in the zones and times of shoshonitic magma formation. Variable water fluxes could be tentatively attributed to different stages of subduction process. Noting that shoshonitic magmas appear during mature to late stages of volcanism, it is reasonable to postulate a decrease of water flux with time.

### *Pre-metasomatic mantle composition*

Gaining insight into the original composition of the upper mantle beneath the Aeolian Islands is difficult, due to extensive modification produced by metasomatic processes. This is however an important step to a better understanding of mantle source evolution and geodynamic setting in the southern Tyrrhenian Sea. Ellam *et al.* (1988) hypothesized an OIB- to MORB-type composition for pre-metasomatic mantle, and suggested that HFSE enrichment in some islands was evidence for the occurrence of the OIB component in the sub-arc mantle. Such a hypothesis also explains the linear Pb-isotope arrays between the Calabro–Peloritano basement and the OIB-type Etna volcano (Fig. 15.6b), which suggest contamination of an OIB-type source by subducted crustal material. By contrast, Francalanci *et al.* (2007) and Tommasini *et al.* (2007) envisage a homogeneous MORB-type pre-metasomatic mantle along the entire arc, and explain the regional geochemical and isotopic variations as entirely related to variable roles of aqueous and supercritical fluids or melts from an altered oceanic crust and associated sediments. Accordingly, radiogenic Pb-isotope signatures observed in some islands were explained as the result of metasomatism by fluids released from sediments and aged Ionian oceanic crust.

The data and discussion presented in this paper support the hypothesis of a zoned OIB- to MORB-type pre-metasomatic mantle for the Aeolian arc. In particular, an OIB-type component in the marginal islands would explain both high HFSE contents and LREE abundances and fractionation. Variable HFSE ratios are also better explained by pre-metasomatic mantle heterogeneities, since these elements behave as immobile during metasomatism.

Francalanci *et al.* (2007) argued that the OIB-type nature of the external islands conflicts with the low Pb-isotope ratios of Alicudi and Stromboli, as compared to those of the central island of Salina. However, relatively unradiogenic Pb compositions at Stromboli are an effect of contamination of the mantle source by sediments, which completely altered its original Pb-isotope signature. A decrease of $^{206}Pb/^{204}Pb$ ratios from Salina to Alicudi is only observed if the Alicudi basalts are considered as the most primitive compositions in the island. However, it has long been demonstrated that the Alicudi basalts are more contaminated than the associated andesites (Peccerillo & Wu 1992; Lucchi *et al.* 2013*a*). Therefore, if more evolved but uncontaminated andesites are considered, Pb-isotopic values at Alicudi are similar to those at Salina.

## Geodynamic implications

There are important relationships between magma and mantle compositions and the geodynamic setting of the Aeolian arc. The diversity of the mantle contamination processes in the western-central and eastern sectors suggests a different nature for the subducted material. A basaltic slab, with little or no sediment involvement, is indicated by geochemical data as a source of metasomatic fluids in the western-central islands, whereas an important contribution by subducted sediments or other upper crustal materials is required for metasomatism at Stromboli. The Tindari–Letojanni Fault therefore represents the boundary that divides two distinct compositions of the subducted material. Such a conclusion is also suggested by Doglioni *et al.* (2001), although these authors propose a continental-type crust in the west and an oceanic-type crust in the east, a conclusion that strongly contrasts with radiogenic isotope signatures of the Aeolian magmas.

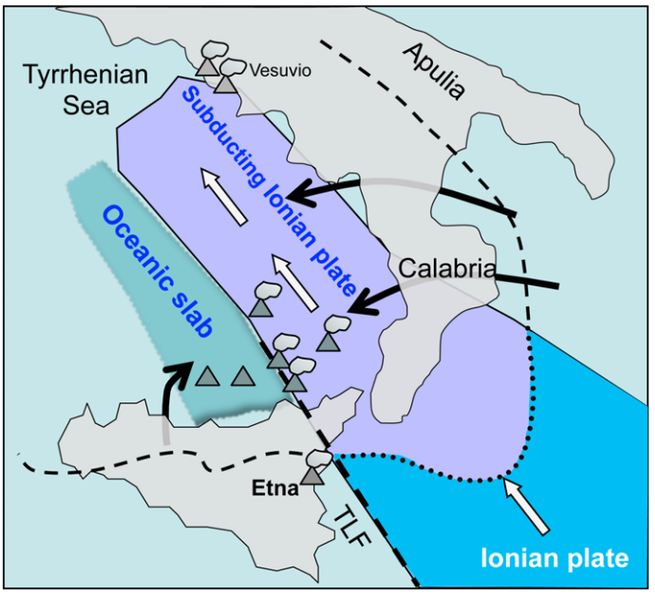


**Fig. 15.12.** Schematic geodynamic setting of the Aeolian arc. A narrow Ionian plate is subducting beneath Calabria and the southern Tyrrhenian Sea. This is associated with deep seismicity and active volcanism, and is bounded to the west by the Tintari–Letojanni Fault (TLF) system. A detached and passively sinking oceanic slab is envisaged for the western Aeolian arc. Curved black arrows indicate asthenospheric mantle inflow from the foreland around the margins of the subducted slabs. Collision zones are indicated with a dashed line. For further explanation, see text.

Metasomatic fluids activated extensive modification of the upper mantle beneath the Aeolian volcanic arc. However, some geochemical signatures of the pre-metasomatic mantle were preserved, and indicate a depleted MORB-type source in the central sector and a more fertile OIB-type component for the external islands.

Peccerillo (2001) argued that the OIB-type component at Stromboli could have originated by inflow of asthenospheric mantle from the Africa foreland around the margins of the retreating slab. Trua *et al.* (2004, 2011) envisaged the same type of process to explain the occurrence of MORB and OIB components at Marsili. Francalanci *et al.* (2007) and Tommasini *et al.* (2007) consider the hypothesis of mantle flow as unrealistic, a statement that does not take into account the particular geodynamic setting of the Aeolian arc. Here, a narrow Ionian slab is subducting beneath the southern Tyrrhenian Sea (Fig. 15.12) and is retreating toward the SE (Gvirtzman & Nur 1999), generating deep seismic activity beneath the eastern Aeolian arc. In contrast, deep seismicity is lacking beneath the western Aeolian arc, a feature that could be related to collision and slab break-off in this sector where a fragment of oceanic slab is suggested to passively sink into the upper mantle (see Peccerillo 2005; Panza *et al.* 2007 for further details).

It is well known that the Benioff zone rollback requires mantle flow to replace the space left by the retreating slab. Such a replacement can occur by mantle flow from the back-arc area. However, for a narrow slab such as that in the southern Tyrrhenian Sea most of the asthenospheric inflow likely occurs from the foreland, moving around the margins of the retreating slab (Fig. 15.12). The mantle sources at the margins of the slab are therefore the most heavily affected by inflow and consequently show the clearest evidence of OIB-type components. It should be recalled that all volcanoes situated on the margin of the African plate (e.g. Etna, Iblei, Linosa, etc.) have an OIB-type composition.

## Conclusions

The overall petrological and geochemical features of the Aeolian arc and the relationships with petrogenesis and geodynamics can be summarized as follows.

(1) CA and HKCA rocks make up all the western islands and the largest part of Lipari and Panarea, whereas HKCA and SHO rocks are dominant at Vulcano and Stromboli. Shoshonitic rocks from these islands have similar compositions for many major and many trace elements, but exhibit strong differences for radiogenic isotopes (Sr–Nd–Pb) and some trace element abundances and ratios. This suggests that shoshonitic magmatism in the Aeolian arc is polygenetic. In particular, decreasing degrees of partial melting of a homogeneous source at various depths generated the transition from high-K calc-alkaline to shoshonitic magmatism at Vulcano. At Stromboli, calc-alkaline and shoshonitic magmas are related to polybaric melting of heterogeneous mantle sources that were variably contaminated by subducted sediments.

(2) There are distinct Sr-, Nd- and Pb-isotope signatures in different sectors of the arc. Some incompatible trace element ratios also show diverging variation trends. Different types of mantle metasomatic processes have been responsible for these features. Metasomatic fluids affecting the western-central arc originated from a subducted basaltic crust, whereas upper crustal material (likely oceanic-type crust plus sediments) was a main source of metasomatic fluids under Stromboli.

(3) Modification by metasomatic fluids was superimposed on a heterogeneous OIB- to MORB-type pre-metasomatic mantle wedge. An OIB-type component in the source is recognized for the external islands of Alicudi and Stromboli and for the Marsili seamount, but not in the central Aeolian arc where a depleted MORB-type mantle composition is suggested by rock chemistry. The OIB-type component was provided by asthenospheric inflow from the Africa foreland, around the edges of the slab during rollback.

(4) Aeolian arc magmas were affected by complex evolution processes which drove parental basalts towards intermediate and acidic compositions. The degree of magma evolution was much more extensive in the central islands of Lipari and Vulcano, where abundant rhyolites were erupted during the latest activity stages. This is related to the transtensional tectonics along the Tindari–Letojanni transfer fault, which favoured the formation of large intra-crustal magma chambers where magmas ponded and fractionated for a long time to give abundant rhyolitic melts.

(5) Geobarometric investigations revealed polybaric magma evolution processes for the Aeolian volcanoes. Early basaltic activity, which characterized the lowest exposed sequences on most islands, was fed by deep magma chambers in which magmatic evolution was dominated by fractional crystallization and assimilation plus continuous mixing with fresh mafic melts from the source. Younger andesitic and rhyolitic activity was fed by shallower magma chambers, where magmatic evolution was dominated by fractional crystallization. An overall upwards migration for magma chambers of the Aeolian volcanoes is therefore suggested by geobarometric investigations.

Research on Aeolian orogenic magmatism has been financed by MIUR, PRIN2008. The authors thank J. Hermann, ANU, R. Harmon and an anonymous referee for constructive reviews.

## References

Barberi, F., Gandino, A., Gioncada, A., La Torre, P., Sbrana, A. & Zenucchini, C. 1994. The deep structure of the Aeolian arc in the light of gravity, magnetic and volcanological data. *Journal of Volcanology and Geothermal Research*, **61**, 189–206.

Barker, D. S. 1987. Rhyolites contaminated with metapelite and gabbro, Lipari, Aeolian Islands, Italy: products of lower crustal fusion or of assimilation plus fractional crystallization? *Contribution to Mineralogy and Petrology*, **97**, 460–472.

Becker, H., Jochum, K. P. & Carlson, R. W. 2000. Trace element fractionation during dehydration of eclogites from high-pressure terranes and the implications for element fluxes in subduction zones. *Chemical Geology*, **163**, 65–99.

Brenan, J. M., Shaw, H. F., Ryerson, F. J. & Phinney, D. L. 1995. Mineral–aqueous fluid partitioning of trace elements at 900 °C and 2 GPa: constraints on the trace element chemistry of mantle and deep crustal fluids. *Geochimica et Cosmochimica Acta*, **59**, 3331–3350.

Calanchi, N., Peccerillo, A. *et al.* 2002. Petrology and geochemistry of the Island of Panarea: implicationsfor mantle evolution beneath the Aeolian island arc (Southern Tyrrhenian Sea, Italy). *Journal of Volcanology and Geothermal Research*, **115**, 367–395.

Crisci, G. M., De Rosa, R., Esperança, S., Mazzuoli, R. & Sonnino, M. 1991. Temporal evolution of a three component system: the island of Lipari (Aeolian Arc, southern Italy). *Bulletin of Volcanology*, **53**, 207–221.

Davì, M., Behrens, H., Vetere, F. & De Rosa, R. 2008. The viscosity of latitic melts from Lipari (Aeolian Islands, Italy): inference on mixing–mingling processes in magmas. *Chemical Geology*, **259**, 89–97.

De Astis, G., La Volpe, L., Peccerillo, A. & Civetta, L. 1997. Volcanological and petrological evolution of Vulcano Island (Aeolian Arc, southern Tyrrhenian Sea). *Journal of Geophysical Research*, **102**, 8021–8050.

De Astis, G., Peccerillo, A., Kempton, P. D., La Volpe, L. & Wu, T. W. 2000. Transition from calc-alkaline to potassium-rich magmatism in subduction environments: geochemical and Sr, Nd, Pb isotopic constraints from the Island of Vulcano (Aeolian arc). *Contributions of Mineralogy and Petrology*, **139**, 684–703.

De Astis, G., Lucchi, F., Dellino, P., La Volpe, L., Tranne, C. A., Frezzotti, M. L. & Peccerillo, A. 2013. Geology, volcanic history and petrology of Vulcano (central Aeolian archipelago). *In*: Lucchi, F., Peccerillo, A., Keller, J., Tranne, C. A. & Rossi, P. L. (eds) *The Aeolian Islands Volcanoes*. Geological Society, London, Memoirs, **37**, 281–348.

De Rosa, R. & Sheridan, M. F. 1983. Evidence for magma mixing in the surge deposits of the Monte Guardia sequence, Lipari. *Journal of Volcanology and Geothermal Research*, **17**, 313–328.

Di Martino, C., Frezzotti, M. L., Lucchi, F., Peccerillo, A., Tranne, C. A. & Diamond, L. W. 2010. Magma storage and ascent at Lipari Island (Aeolian archipelago, southern Italy) during the old stages (223–81 ka): role of crustal processes and tectonic influence. *Bulletin of Volcanology*, **72**, 1061–1076.

Di Martino, C., Forni, F. *et al.* 2011. Formation of cordierite-bearing lavas during anatexis in the lower crust beneath Lipari Island (Aeolian arc, Italy). *Contribution to Mineralogy and Petrology*, **162**, 1011–1030.

Dietrich, V., Emmermann, R., Keller, J. & Puchelt, H. 1977. Tholeiitic basalts from the Tyrrhenian Sea floor. *Earth and Planetary Science Letters*, **36**, 285–296.

Doglioni, C., Innocenti, F. & Mariotti, G. 2001. Why Mt. Etna? *Terra Nova*, **13**, 25–31.

Ellam, R. M. & Harmon, R. S. 1990. Oxygen isotope constraints on the crustal contribution to the subduction-related magmatism of the Aeolian Islands, southern Italy. *Journal of Volcanology and Geothermal Research*, **44**, 105–122.

Ellam, R. M., Menzies, M. A., Hawkesworth, C. J., Leeman, W. P., Rosi, M. & Serri, G. 1988. The transition from calc-alkaline to potassic orogenic magmatism in the Aeolian Islands, Southern Italy. *Bulletin of Volcanology*, **50**, 386–398.

Ellam, R. M., Hawkesworth, C. J., Menzies, M. A. & Rogers, N. W. 1989. The volcanism of Southern Italy: role of subducion and the relationships between potassic and sodic alkaline magmatism. *Journal of Geophysical Research*, **94**, 4589–4601.

Elliott, T., Plank, T., Zindler, A., White, W. & Bourdon, B. 1997. Element transport from slab to volcanic front at the Mariana arc. *Journal of Geophysical Research*, **102**, 14991–15019.

Esperança, S., Crisci, G. M., De Rosa, R. & Mazzuoli, R. 1992. The role of the crust in the magmatic evolution of the Island of Lipari (Aeolian Islands, Italy). *Contributions to Mineralogy and Petrology*, **112**, 450–462.

Forni, F., Lucchi, F., Peccerillo, A., Tranne, C. A., Rossi, P. L. & Frezzotti, M. L. 2013. Stratigraphy and geological evolution of the Lipari volcanic complex (central Aeolian archipelago). *In*: Lucchi, F., Peccerillo, A., Keller, J., Tranne, C. A. & Rossi, P. L. (eds) *The Aeolian Islands Volcanoes*. Geological Society, London, Memoirs, **37**, 213–280.

Francalanci, L., Barbieri, M., Manetti, P., Peccerillo, A. & Tolomeo, L. 1988. Sr isotopic systematics in volcanic rocks from the Island of Stromboli, Aeolian arc (Italy). *Chemical Geology (Isotope Geoscience Section)*, **73**, 109–124.

Francalanci, L., Manetti, P. & Peccerillo, A. 1989. Volcanological and magmatological evolution of Stromboli volcano (Aeolian Islands): the roles of fractional crystallization, magma mixing, crustal contamination, and source heterogeneity. *Bulletin of Volcanology*, **51**, 355–378.

Francalanci, L., Taylor, S. R., Mcculloch, M. T. & Woolhead, J. D. 1993. Geochemical and isotopic variations in the calc-alkaline rocks of Aeolian arc, southern Tyrrhenian Sea, Italy: constraints on magma genesis. *Contributions to Mineralogy and Petrology*, **113**, 300–313.

Francalanci, L., Avanzinelli, R., Petrone, C. M. & Santo, A. 2004. Petrochemical and magmatological characteristics of the Aeolian Arc volcanoes, southern Tyrrhenian Sea, Italy: inferences on shallow level processes and magma source variations. *Periodico di Mineralogia*, **73**, 75–104.

Francalanci, L., Avanzinelli, R., Tommasini, S. & Heuman, A. 2007. A west-east geochemical and isotopic traverse along the volcanism of the Aeolian Island arc, southern Tyrrhenian Sea, Italy: interferences on mantle source processes. *Geological Society of America Special Papers*, **418**, 235–263.

Francalanci, L., Lucchi, F., Keller, J., De Astis, G. & Tranne, C. A. 2013. Eruptive, volcano-tectonic and magmatic history of the Stromboli volcano (north-eastern Aeolian archipelago). *In*: Lucchi, F., Peccerillo, A., Keller, J., Tranne, C. A. & Rossi, P. L. (eds) *The Aeolian Islands Volcanoes*. Geological Society of London, Memoirs, **37**, 395–470.

Frezzotti, M. L. & Peccerillo, A. 2004. Fluid inclusion and petrological studies elucidate reconstruction of magma conduits. *Transactions of the American Geophysical Union*, **85**, 157.

Frezzotti, M. L., Peccerillo, A. & Bonelli, R. 2003. Magma ascent rates and depths of magma reservoirs beneath the Aeolian volcanic arc (Italy): inferences from fluid and melt inclusions in crustal xenoliths. *In*: Bodnar, B. & De Vivo, B. (eds) *Melt Inclusions in Volcanic Systems*. Elsevier, Amsterdam, 185–206.

Frezzotti, M. L., Peccerillo, A., Zanon, V. & Nikogosian, I. 2004. Silica-rich melts in quartz xenoliths from Vulcano island and their bearing on process of crustal anatexis and crust-magma interaction beneath the Aeolian arc, southern Italy. *Journal of Petrology*, **45**, 3–26.

Gertisser, R. & Keller, J. 2000. From basalt to dacite: origin and evolution of the calc-alkaline series of Salina, Aeolian Arc, Italy. *Contributions to Mineralogy and Petrology*, **139**, 607–626.

Gillot, P. Y. 1987. Histoire volcanique des Iles Eoliennes: arc insulaire ou complexe orogénique anulaire? *Documents et Travaux, Institut Géologique Albert-de-Lapparent,* Paris, **11**, 35–42.

Gioncada, A., Mazzuoli, R., Bisson, M. & Pareschi, M. T. 2003. Petrology of volcanic products younger than 42 ka on the Lipari-Vulcano complex (Aeolian Islands, Italy): an example of volcanism controlled by tectonics. *Journal of Volcanology and Geothermal Research*, **122**, 191–220.

Gioncada, A., Mazzuoli, R. & Milton, A. J. 2005. Magma mixing at Lipari (Aeolian Islands, Italy): insights from textural and compositional features of phenocrysts. *Journal of Volcanology and Geothermal Research*, **145**, 97–118.

Grasso, M. 2001. The Apenninic-Maghrebian orogen in Southern Italy, Sicily and adjacent areas. *In*: Vai, G. B. & Martini, P. I. (eds) *Anatomy of an Orogen. The Apennines and adjacent Mediterranean basins*. Kluwer, Dordrecht, 255–286.

Grove, T. L., Till, C. B. & Krawczynsky, M. J. 2012. The role of $H_2O$ in subduction-zone magmatism. *Annual Review of Earth and Planetary Science*, **40**, 413–439.

Gvirtzman, Z. & Nur, A. 1999. The formation of Mount Etna as the consequence of slab rollback. *Nature*, **401**, 782–785.

Hart, S. R. 1984. A large-scale isotope anomaly in the Southern Hemisphere mantle. *Nature*, **309**, 753–757.

Hart, S. R., Hauri, E. H., Oschmann, L. A. & Whitehead, J. A. 1992. Mantle plumes and entrainment—Isotopic evidence. *Science*, **256**, 517–520.

Hermann, J. & Rubatto, D. 2009. Accessory phase control on trace element signature of sediment melt in subduction zones. *Chemical Geology*, **265**, 512–526.

Keller, J. 1982. The Mediterranean island arc. *In*: Thorpe, R. S. (ed.) *Andesites: Orogenic Andesites and Related Rocks*. Wiley, Chichester, 307–325.

Kessel, R., Schmidt, M. W., Ulmer, P. & Pettke, T. 2005. Trace element signatures of subduction-zone fluids, melts and supercritical liquids at 120–180 km depth. *Nature*, **437**, 724–727.

Leocat, E. 2011. *Histoire eruptive des volcans du secteur occidental des Iles Eoliennes (Sud de la Mer Tyrrhenienne, Italie). PhD thesis*, University of Paris Sud, Orsay.

Lucchi, F., Peccerillo, A., Tranne, C. A., Rossi, P. L., Frezzotti, M. L. & Donati, C. 2013*a*. Volcanism, calderas and magmas of the Alicudi composite volcano (western Aeolian archipelago). *In*: Lucchi, F., Peccerillo, A., Keller, J., Tranne, C. A. & Rossi, P. L. (eds) *The Aeolian Islands Volcanoes*. Geological Society, London, Memoirs, **37**, 83–112.

Lucchi, F., Santo, A. P., Tranne, C. A., Peccerillo, A. & Keller, J. 2013*b*. Volcanism, magmatism, volcano-tectonics and sea-level fluctuations in the geological history of Filicudi (western Aeolian archipelago). *In*: Lucchi, F., Peccerillo, A., Keller, J., Tranne, C. A. & Rossi, P. L. (eds) *The Aeolian Islands Volcanoes*. Geological Society, London, Memoirs, **37**, 113–154.

Lucchi, F., Gertisser, R., Keller, J., Forni, F., De Astis, G. & Tranne, C. A. 2013*c*. Eruptive history and magmatic evolution of the Island of Salina (central Aeolian archipelago). *In*: Lucchi, F., Peccerillo, A., Keller, J., Tranne, C. A. & Rossi, P. L. (eds) *The Aeolian Islands Volcanoes*. Geological Society, London, Memoirs, **37**, 155–212.

Lucchi, F., Tranne, C. A., Peccerillo, A., Keller, J. & Rossi, P. L. 2013*d*. Geological history of the Panarea volcanic group (eastern Aeolian archipelago). *In*: Lucchi, F., Peccerillo, A., Keller, J., Tranne, C. A. & Rossi, P. L. (eds) *The Aeolian Islands Volcanoes*. Geological Society, London, Memoirs, **37**, 349–394.

Martelli, M., Nuccio, P. M., Stuart, F. M., Di Liberto, V. & Ellam, R. M. 2008. Constraints on mantle source and interactions from He-Sr isotope variation in Italian Plio-Quaternary volcanism. *Geochemistry, Geophysics, Geosystems*, **9**, Q02001, doi: 10.1029/2007GC001730.

Nazzareni, S., Molin, G., Peccerillo, A. & Zanazzi, P. F. 1998. Structural and chemical variations in clinopyroxenes from the Island of Alicudi (Aeolian arc) and their implications for conditions of crystallization. *European Journal of Mineralogy*, **10**, 291–300.

Nazzareni, S., Molin, M., Peccerillo, A. & Zanazzi, P. F. 2001. Volcanological implications of crystal chemical variations in clinopyroxenes from the Aeolian arc (Southern Tyrrhenian Sea, Italy). *Bulletin of Volcanology*, **63**, 73–82.

Nicolosi, I., Speranza, F. & Chiappini, M. 2006. Ultrafast oceanic spreading of the Marsili basin, southern Tyrrhenian Sea: evidence from magnetic anomaly analysis. *Geology*, **34**, 717–720.

O'hara, M. J. 1977. Geochemical evolution during fractional crystallization of a periodically refilled magma chamber. *Nature*, **266**, 503–507.

Panza, G. F., Pontevivo, A., Chimera, G., Raykova, R. & Aoudia, A. 2003. The lithosphere-asthenosphere: Italy and surroundings. *Episodes*, **26**, 169–174.

Panza, G. F., Peccerillo, A., Aoudia, A. & Farina, B. 2007. Geophysical and petrological modelling of the upper mantle structure and composition: the case of the Tyrrhenian Sea area. *Earth Science Reviews*, **80**, 1–46.

Peccerillo, A. 2001. Geochemical similarities between the Vesuvius, Phlegraean Fields and Stromboli volcanoes: petrogenetic, geodynamic and volcanological implications. *Mineralogy and Petrology*, **73**, 93–105.

Peccerillo, A. 2005. *Plio-Quaternary Volcanism in Italy. Petrology, Geochemistry, Geodynamics*. Springer, Heidelberg.

Peccerillo, A. & Taylor, S. R. 1976. Geochemistry of the Eocene calc-alkaline volcanic rocks from the Kastamonu area, northern Turkey. *Contributions to Mineralogy and Petrology*, **58**, 63–81.

Peccerillo, A. & Wu, T. W. 1992. Evolution of calc-alkaline magmas in continental arc volcanoes: evidence from Alicudi, Aeolian Arc (Southern Tyrrhenian Sea, Italy). *Journal of Petrology*, **33**, 1295–1315.

Peccerillo, A., Kempton, P. D., Harmon, R. S., Wu, T. W., Santo, A. P., Boyce, A. J. & Tripodo, A. 1993. Petrological and geochemical characteristics of the Alicudi Volcano, Aeolian Island, Italy: implication for magma genesis and evolution. *Acta Vulcanologica*, **3**, 235–249.

Peccerillo, A., Dallai, L., Frezzotti, M. L. & Kempton, P. D. 2004. Sr-Nd-Pb-O isotopic evidence for decreasing crustal contamination with ongoing magma evolution at Alicudi volcano (Aeolian Arc, Italy): implication for style of magma-crust interaction and mantle source compositions. *Lithos*, **78**, 217–233.

Peccerillo, A., Frezzotti, M. L., De Astis, G. & Ventura, G. 2006. Modeling the magma plumbing system of Vulcano (Aeolian Islands, Italy) by integrated fluid-inclusion geobarometry, petrology and geophysics. *Geology*, **34**, 17–20.

Perugini, D., Ventura, G., Petrelli, M. & Poli, G. 2004. Kinematic significance of morphological structures generated by mixing of magmas: a case study from Salina Island (southern Italy). *Earth and Planetary Science Letters*, **222**, 1051–1066.

Perugini, D., Valentini, L. & Poli, G. 2007. Insights into Magma Chamber Processes from the Analysis of Size Distribution of Enclaves in Lava Flows: a Case Study from Vulcano Island (Southern Italy). *Journal of Volcanology and Geothermal Research*, **166**, 193–203.

Petrelli, M., Perugini, D., Poli, G. & Peccerillo, A. 2007. Graphite electrode lithium tetraborate fusion for trace element determination in bulk geological samples by laser ablation ICP-MS. *Microchimica Acta*, **158**, 275–282, doi: 10.1007/s00604-006-0731-6.

Petrelli, M., Perugini, D., Alagna, K. E., Poli, G. & Peccerillo, A. 2008. Spatially resolved and bulk trace element analysis by laser ablation – inductively coupled plasma – mass spectrometry (LA-ICP-MS). *Periodico di Mineralogia*, **77**, 3–21.

Piochi, M., De Astis, G., Petrelli, M., Ventura, G., Sulpizio, R. & Zanetti, A. 2009. Constraining the recent plumbing system of Vulcano (Aeolian Arc, Italy) by textural, petrological, and fractal analysis: the 1739 A.D. Pietre Cotte lava flow. *Geochemistry, Geophysics, Geosystems*, **10**, Q01009, doi: 10.1029/2008GC002176.

Rottura, A., Del Moro, A. *et al.* 1991. Relationships between intermediate and acidic rocks in orogenic granitoids suites: petrological, geochemical and isotopic (Sr, Nd, Pb) data from Capo Vaticano (southern Calabria, Italy). *Chemical Geology*, **92**, 153–176.

Santo, A. P. & Peccerillo, A. 2008. Oxygen isotopic variations in the clinopyroxenes from the Filicudi volcanic rocks (Aeolian Islands, Italy): implications for open-system magma evolution. *Open Mineralogy Journal*, **2**, 1–12.

Santo, A. P., Jacobsen, S. B. & Baker, J. 2004. Evolution and genesis of calc-alkaline magmas at Filicudi volcano, Aeolian Arc (Southern Tyrrhenian Sea, Italy). *Lithos*, **72**, 73–96.

Schiavi, F., Kobayashi, K., Nakamura, E., Tiepolo, M. & Vannucci, R. 2012. Trace element and Pb-B-Li isotope systematics of olivine-hosted melt inclusions: insught into metasomatism beneath Stromboli (southern Italy). *Contributions to Mineralogy and Petrology*, **163**, 1011–1031.

Sun, S.-S. & Mcdonough, W. F. 1989. Chemical and isotopic systematics of oceanic basalts: implications for mantle composition and processes. *In*: Saunders, A. D. & Norry, M. J. (eds) *Magmatism in the Ocean Basins*. Geological Society, London, Special Publications, **42**, 313–345.

Tommasini, S., Heumann, A., Avanzinelli, R. & Francalanci, L. 2007. The fate of high-angle dipping slabs in the subduction factory: an integrated trace element and radiogenic isotope (U, Th, Sr, Nd, Pb) study of Stromboli Volcano, Aeolian Arc, Italy. *Journal of Petrology*, **48**, 2407–2430.

Tonarini, S., Leeman, W. P., Civetta, L., D'antonio, M., Ferrara, G. & Necco, A. 2004. B/Nb and $\delta^{11}$B systematics in the Phlegrean Fields District, Italy. *Journal of Volcanology and Geothermal Research*, **133**, 123–139.

Trua, T., Serri, G., Marani, M. P., Rossi, P. L., Gamberi, F. & Renzulli, A. 2004. Mantle domains beneath the southern Tyrrhenian: constraints from recent seafloor sampling and dynamic implications. *Periodico di Mineralogia*, **73**, 53–73.

Trua, T., Marani, M. P. & Gamberi, F. 2011. Magmatic evidence for African mantle propagation into the southern Tyrrhenian backarc region. *In*: Beccaluva, L., Bianchini, G. & Wilson, M. (eds) *Volcanism and Evolution of the African Lithosphere*. Geological Society of America, Boulder, Special Paper **478**, 307–331.

Ulmer, P. 2001. Partial melting in the mantle wedge – The role of $H_2O$ in the genesis of mantle-derived 'arc-related' magmas. *Physics of Earth and Planetary Interior*, **127**, 215–232.

Ventura, G. 2013. Kinematics of the Aeolian volcanism (Southern Tyrrhenian Sea) from geophysical and geological data. *In*: Lucchi, F., Peccerillo, A., Keller, J., Tranne, C. A. & Rossi, P. L. (eds) *The Aeolian Islands Volcanoes*. Geological Society, London, Memoirs, **37**, 3–12.

Viccaro, M. & Cristofolini, R. 2008. Nature of mantle heterogeneity and its role in the short-term geochemical and volcanological evolution of Mt. Etna (Italy). *Lithos*, **105**, 272–288.

Wilson, M. & Downes, H. 1991. Tertiary-Quaternary extension-related alkaline magmatism in Western and Central Europe. *Journal of Petrology*, **32**, 811–849.

Zanon, V., Frezzotti, M. L. & Peccerillo, A. 2003. Magmatic feeding system and crustal magma accumulation beneath Vulcano Island (Italy): evidence from $CO_2$ fluid inclusions in quartz xenoliths. *Journal of Geophysical Research*, **108**, 2298–2301.

Zindler, A. & Hart, S. 1986. Chemical geodynamcs. *Annual Review of Earth and Planetary Sciences*, **14**, 493–571.